ORIGINAL RESEARCH ARTICLE

Phosphorus Enrichment Capacity of Calcium Silicates in Multiphase Dephosphorization Slag Based on Laboratory High Temperature Experiments and IMCT

HAN SUN, WEN-KUI YANG, RUN-HAO ZHANG, and JIAN YANG

The present work aims to study the phosphorus enrichment capacity of four kinds of calcium silicate in multiphase dephosphorization slag under different process parameters by combining laboratory high temperature experiment and ion–molecule coexistence theory (IMCT). The results show that the dephosphorization ratio is enhanced by increasing the slag basicity, Fe_2O_3 addition amount and dephosphorization time. With increasing temperature and initial P content of hot metal, dephosphorization ratio increases first and then decreases. The phosphorus enrichment contribution ratios R_{Ci} of CS and C_2S accounts for more than 95 pct in multiphase dephosphorization slag. The R_{CS} is positively related to temperature, Fe_2O_3 addition amount, initial P content of hot metal and time in varying degrees, while negatively related to the slag basicity. The change rule of R_{C_2S} is opposite to that of R_{CS}. Within the research range of respective process parameters, the transformation nodes of the phosphorus enrichment degree of CS–C_3P and C_2S–C_3P in multiphase dephosphorization slag are as follows: the slag basicity is 1.45, the Fe_2O_3 addition amount is 19.55 g, the initial P content of hot metal is 0.182 pct and the reaction time is 8.46 minutes. The phosphorus enrichment degree of C_2S–C_3P is always higher than that of CS–C_3P in the temperature range of 1300 °C to 1450 °C. The consistency between the phosphorus enrichment capacity of calcium silicate calculated based on IMCT and the coefficient n of C_nS–C_3P estimated based on laboratory experimental measurement results is verified.

https://doi.org/10.1007/s11663-023-02790-9

I. INTRODUCTION

REDUCING the generation and discharge amount of steelmaking slag effectively is one of the methods to achieve clean green metallurgy.[1,2] New double slag converter steelmaking process (NDSP) is an improved converter steelmaking process proposed in recent years, which adds auxiliary materials through material balance quantitative calculation and combines multi gun position and multi-stage blowing.[3,4] The advantage of NDSP is that the solid–liquid coexisting low basicity multiphase slag formed in the dephosphorization stage can effectively promote the dephosphorization of hot metal, and the slag recycling can significantly reduce the lime consumption and the carbon dioxide emission during the converter steelmaking.[3,4] Therefore, the NDSP with the characteristics of green metallurgy and clean steel production is a process with great development potential among various pyrometallurgical converter steelmaking processes.

Due to the reduction of lime addition amount, the phosphorus enrichment capacity of the solid–liquid coexisting multiphase dephosphorization slag formed in the dephosphorization stage of NDSP needs to be further studied.[5] In order to clarify the dephosphorization behavior of hot metal and the phosphorus enrichment capacity of slag in dephosphorization stage of NDSP under complex process conditions, some scholars have conducted researches on dephosphorization of hot metal at low temperature and low slag basicity through laboratory high temperature experiments or industrial experiments.[3,4,6–36] Table I extensively collects the researches on dephosphorization behavior of hot metal and phosphorus enrichment capacity of slag under low temperature and low basicity conditions based on

HAN SUN, WEN-KUI YANG, RUN-HAO ZHANG, and JIAN YANG are with the State Key Laboratory of Advanced Special Steel, School of Materials Science and Engineering, Shanghai University, Shanghai 200444, P.R. China. Contact e-mails: yangwenkui@shu.edu.cn; yang_jian@t.shu.edu.cn.

Manuscript submitted January 13, 2023; accepted March 24, 2023. Article published online May 16, 2023.

Table I. Main Works of Dephosphorization Behavior of Hot Metal and Phosphorus Enrichment Capacity of Slag Under the Low Temperature and Low Slag Basicity Based on Laboratory High Temperature Experiments or Industrial Experiments in the Past 5 Years

Author	Experiment	Method	Main Work	Year	References
Wang *et al.*	industrial experiment	statistical analysis of data	influence of temperature, slag basicity, oxygen blowing pressure and reaction time on dephosphorization ratio of hot metal in dephosphorization stage of double slag steelmaking process	2018	[6]
Xie *et al.*	laboratory experiment	thermodynamic calculation	Clarify the dissolution behavior of solid CaO and the phosphorus enrichment capacity of calcium silicate in multiphase slag based on the ion–molecule coexistence theory (IMCT)	2018	[7]
Uchida *et al.*	laboratory experiment	SEM–EDS; phase diagram	effect of slag basicity on the formation of P-rich phase in steelmaking slag	2018	[8]
Xie *et al.*	laboratory experiment	SEM–EDS; FT-IR	effect of Al_2O_3 content on the melting point, viscosity and phosphorus distribution ratio of $CaO–SiO_2–Fe_2O_3–P_2O_5$ slag	2018	[9]
Li *et al.*	laboratory experiment	SEM–EDS; kinetic model	isothermal crystallization behavior of P-rich phase in rapidly quenched $CaO–SiO_2–FeO–Fe_2O_3–P_2O_5$ steelmaking slag under different cooling systems	2018	[10]
Li *et al.*	industrial experiment	thermodynamic calculation	establish a thermodynamic model to predict the phosphorus distribution ratio between $CaO–SiO_2–MgO–FeO–Fe_2O_3–Al_2O_3–P_2O_5$ slag and molten steel based on IMCT	2019	[11]
Su *et al.*	laboratory experiment	SEM–EDS; statistical analysis of data	effect of Na_2O addition amount (0 to 15 pct) on P_2O_5 distribution between solid solution and matrix phase	2019	[12]

Table I. continued

Author	Experiment	Method	Main Work	Year	References
Wang *et al.*	industrial experiment	statistical analysis of data	comparison between double slag steelmaking process and single slag steelmaking process on dephosphorization results of hot metal under different slag basicity, Fe_tO content and bath temperature	2019	[13]
Yao *et al.*	laboratory experiment	numerical simulation	dynamic characteristics of 300 t converter based on hydraulic model and numerical simulation. Influence of gas supply mode on decarburization and dephosphorization reaction and the end point carbon–oxygen balance of molten steel	2020	[14]
Silva *et al.*	laboratory experiment	thermodynamic calculation	effects of liquid and solid phase fractions, CaO and FeO activities and slag viscosity on dephosphorization efficiency of hot metal using the FactSage thermodynamic software	2020	[15]
Lin *et al.*	laboratory experiment	thermodynamic calculation; kinetic model	influence of slag temperature on the thermodynamic and kinetic behavior of P-rich phase formation in slag, the existence form and enrichment behavior of phosphorus in slag	2020	[16]
Ye *et al.**	industrial experiment	FESEM; thermodynamic calculation	influence of slag basicity on the dephosphorization behavior of hot metal and phosphorus distribution ratio between slag and molten steel at the end of dephosphorization stage based on the NDSP. Clarify the effect of basicity on P_2O_5 content and the area fraction of P-rich phase in dephosphorization slag	2020	[17]

Table I. continued

Author	Experiment	Method	Main Work	Year	References
Yang *et al.**	laboratory experiment	EPMA; thermodynamic calculation	effect of slag basicity (1.40 to 1.83) on dephosphorization ratio of hot metal, phosphorus distribution ratio between slag and steel and mineral phase compositions of dephosphorization slag	2020	[18]
Yan *et al.*	Laboratory experiment	SEM–EDS, thermodynamic calculation	effect of $CaCl_2$ addition amount on the phosphorus distribution ratio between $CaO–SiO_2–FeO_x–P_2O_5–CaCl_2$ slag and carbon saturated hot metal. Mechanism of $CaCl_2$ addition amount on phosphorus distribution ratio between slag and steel	2021	[19]
de Souza *et al.*	industrial experiment	thermodynamic calculation; statistical analysis of data	effect of temperature, slag viscosity, liquid phase amount, CaO and FeO activity and Si content in hot metal on dephosphorization ratio of molten steel	2021	[20]
Maruoka *et al.*	laboratory experiment	EPMA; phase diagram	propose a new process of producing low phosphorus steel by enriching phosphorus in dicalcium silicate phase through partial reduction method	2021	[21]
Kikuchi *et al.*	laboratory experiment	thermodynamic; kinetics; phase diagram	effect of CaO dissolution rate in slag on dephosphorization of hot metal at low temperature and low basicity	2021	[22]
Yang *et al.**	laboratory experiment	SEM–EDS; thermodynamic calculation	clarify the dephosphorization behavior of hot metal at 1300 °C to 1450 °C and slag basicity of 1.8. Quantitatively analyzed the content of different phosphorus containing solid solutions in P-rich phase of dephosphorization slag	2021	[23]

Table I. continued

Author	Experiment	Method	Main Work	Year	References
Yang *et al.**	laboratory experiment	Raman spectrum; FT-IR; SEM–EDS	study the structure and viscosity of low basicity dephosphorization slag at 1300 °C to 1450 °C	2021	[24]
Sun *et al.**	industrial experiment	SEM–EDS; thermodynamic calculation	effect of dephosphorization endpoint temperature on dephosphorization of hot metal at low temperature and low basicity in NDSP. Clarify the path of phosphorus in hot metal entering the P-rich phase of dephosphorization slag. Predict the optimum deslagging temperature at the end of dephosphorization stage in NDSP	2021	[3]
Sun *et al.**	industrial experiment	SEM–EDS; thermodynamic calculation	influence of slag basicity on the dephosphorization of hot metal and the phosphorus enrichment capacity of dephosphorization slag based on the IMCT and the NDSP. Morphologies of P-rich phase in dephosphorization slag at different basicities	2021	[4]
Yang *et al.**	laboratory experiment	SEM–EDS; thermodynamic calculation	effect of Fe_2O_3 addition amount on dephosphorization of hot metal at 1350 °C. Study the existing form of phosphorus in P-rich phase of dephosphorization slag	2021	[25]
Zhang *et al.**	industrial experiment	kinetic model	develop a kinetic model for dephosphorization stage of NDSP based on the coupled reaction model and heat balance temperature model	2021	[26]

Table I. continued

Author	Experiment	Method	Main Work	Year	References
Zhang *et al.**	industrial experiment	kinetic model	influence of dephosphorization slag basicity on hot metal dephosphorization was discussed based on the developed dephosphorization kinetic model, and element contents of hot metal after dephosphorization predicted by the kinetic model were in good agreement with the industrial experiment results	2021	[27]
Yang *et al.**	Laboratory experiment	Raman spectrum; SEM–EDS; thermodynamic calculation	effect of initial P content (0.057 to 0.292 pct) of hot metal on dephosphorization ability and microstructure of low basicity dephosphorization slag	2021	[28]
Yang *et al.**	Laboratory experiment	Raman spectrum; SEM–EDS; thermodynamic calculation	effect of slag basicity (0.98 to 2.13) on dephosphorization behavior of hot metal, microstructure and mineral phase of dephosphorization slag	2021	[29]
Yang *et al.**	Laboratory experiment	SEM–EDS; statistical analysis of data	change in dephosphorization behavior of hot metal with time by controlling different reaction times in each dephosphorization experiment and taking samples at different reaction times in the same experiment	2021	[30]
Xue *et al.*	Laboratory experiment	thermodynamic calculation; SEM–EDS	design a kind of CaO–SiO_2–Al_2O_3–Fe_2O_3 slag without fluoride addition. The effects of basicity, Fe_2O_3 content and Al content on dephosphorization ratio of hot metal were discussed with FactSage thermodynamic calculation	2021	[31]
Wang *et al.*	laboratory experiment	SEM–EDS; thermodynamic calculation	effects of heat treatment conditions and slag basicity on P_2O_5 content and P-rich phase size in dephosphorization slag	2022	[32]

Table I. continued

Author	Experiment	Method	Main Work	Year	References
Sun *et al.*	laboratory experiment	kinetic model	establish a new dephosphorization kinetic model by introducing the concept of "dynamic relative area", and the accuracy of the new model in predicting the relationship between phosphorus content and time is higher than that of the traditional model	2022	[33]
Zhang *et al.**	industrial experiment; laboratory experiment	kinetic model	220 t industrial experiments and 0.5 kg laboratory experiments were carried out at different temperatures, and the P and Si contents of hot metal predicted by the kinetic model were consistent with the industrial and experimental results	2022	[34]
Sun *et al.*	laboratory experiment	thermodynamic calculation; structural analysis	the mechanism of Ce_2O_3 addition amount on the dephosphorization of $CaO–Al_2O_3–SiO_2–MnO$-based slag was studied with thermodynamic calculation, structural analysis, melting temperature and viscosity experiment	2022	[35]
Sun *et al.**	industrial experiment	thermodynamic calculation; SEM–EDS	influence of dephosphorization endpoint temperature on the dephosphorization behavior of hot metal and the phosphorus enrichment ability of the slag were studied based on the IMCT and the NDSP. Clarify the shape evolution of the P-rich phase in the dephosphorization slag under the conditions of 1345 °C to 1450 °C and slag basicity of about 1.50	2022	[36]

The works with symbol "*" were the previous works of our research team.

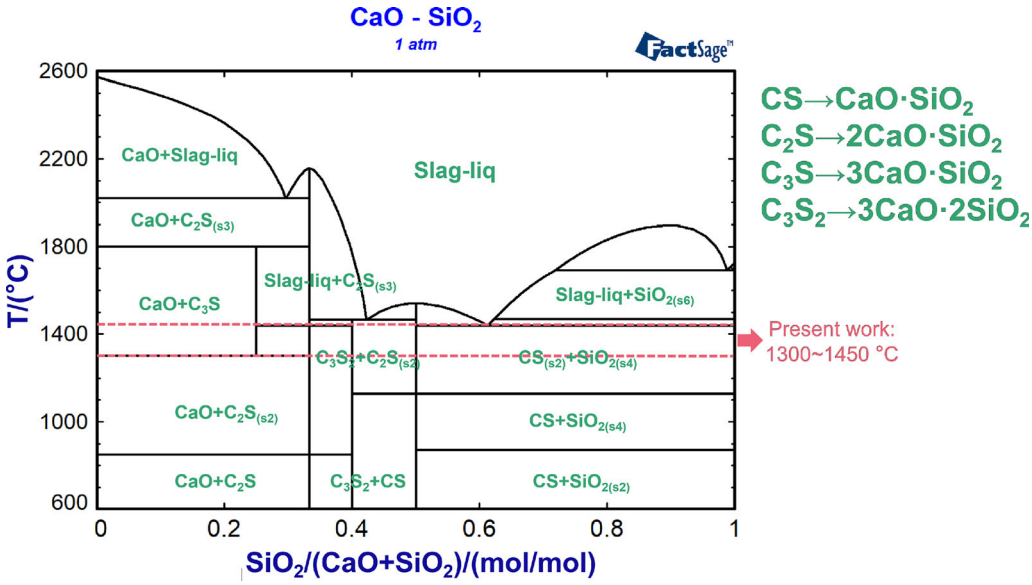

Fig. 1—Standard $CaO–SiO_2$ phase diagram from FactSage8.1 software.

laboratory high temperature experiments or industrial experiments in the past 5 years during 2018 to 2022, and briefly describes the main works of these researches.

According to Table I, thermodynamic calculation and SEM–EDS are usually used to clarify dephosphorization behavior and phosphorus migration mechanism of hot metal under different process parameters.[3,4,7–12,15–19,22–25,28–32,35,36] Kikuchi *et al.*[22] studied the influence of CaO dissolution rate in slag on dephosphorization of hot metal under low temperature and low basicity. Yang *et al.*[24,28,29] clarified the changes of microstructure and properties of dephosphorization slag under different process parameters through Raman spectroscopy and Fourier Transform Infrared (FT-IR) spectrometer. Zhang *et al.*[26] and Sun and Xiang[33] established kinetic models of hot metal dephosphorization suitable for different process conditions, and these models can successfully predict the changes in hot metal compositions with time. However, the quantitative research on the phosphorus enrichment capacity of calcium silicate in low basicity multiphase dephosphorization slag at low temperature is very limited. It is important to clarify the phosphorus enrichment capacity of calcium silicate in multiphase dephosphorization slag under different process parameters for improving the overall dephosphorization ability of converter. Based on the composition data of hot metal and dephosphorization slag under multiple parameters obtained in our previous experiments,[3,4,17,18,23–30,34,36] the phosphorus enrichment ability of calcium silicate in multiphase dephosphorization slag under different process parameters can be systematically evaluated.

According to the classical dephosphorization reaction of hot metal, as shown in Eq. [1]. P at the hot metal side of the slag–hot metal interface will be oxidized by the highly oxidizing slag to form P_2O_5, and react with CaO in the slag to form phosphate, such as $3CaO·P_2O_5$ (C_3P).[37] CaO in slag can react with SiO_2 to form different kinds of calcium silicate, such as $2CaO·SiO_2$ (C_2S), *etc.*[38] P in phosphate can replace the position of Si in some calcium silicate tetrahedrons to form a variety of P_2O_5 containing solid solutions, such as $2CaO·SiO_2–3CaO·P_2O_5$ ($C_2S–C_3P$), which can stably exist in the dephosphorization slag.[39] Figure 1 shows the standard $CaO–SiO_2$ phase diagram from FactSage8.1 software. In the temperature range of dephosphorization stage of NDSP (1300 °C to 1450 °C), there are four kinds of calcium silicate exist in multiphase dephosphorization slag, which are $CaO·SiO_2$ (CS), C_2S, $3CaO·SiO_2$ (C_3S) and $3CaO·2SiO_2$ (C_3S_2), respectively. The different process parameters have influences on the phosphorus enrichment capacity of four kinds of calcium silicate and the solid solutions they form in multiphase dephosphorization slag in different degrees. Zhong *et al.* focused on the equilibrium between molten iron and the mixture of $C_2S–C_3P$ solid solution and CaO at 1550 °C and 1600 °C, and measured the activity of P_2O_5 and C_3P in $C_2S–C_3P$ solid solution in multiphase slag by applying the chemical equilibration method.[40,41] Further, they studied the thermodynamic properties of P_2O_5 in the $C_2S–C_3P$ solid solution saturated with MgO.[42] They found that with increasing C_3P content in the solid solution, the activities of P_2O_5 and $3MgO·P_2O_5$ increase. In addition, the activity of P_2O_5 in the $C_2S–C_3P$ solid solution saturated with MgO is larger than that saturated with CaO.

$$2[P] + 5(FeO) + 3(CaO) = 5[Fe] + (3CaO \cdot P_2O_5). \quad [1]$$

In order to quantitatively evaluate the phosphorus enrichment capacity of four kinds of calcium silicate and the phosphorus enrichment degree of different P_2O_5 containing solid solutions in multiphase dephosphorization slag, the reaction ability of complex molecules formed in slag should be measured or calculated reasonably. How to select an appropriate thermodynamic activity model to further calculate the reaction

ability of slag components needs to be discussed. Table II lists nine activity prediction models of slag components, which have been proposed and summarized elsewhere. The present work comprehensively judges the applicability of these prediction models to calculate the activity of simple oxide, silicate and P_2O_5 containing solid solution in slag, as shown in Table II.

Compared with the other eight activity prediction models, the IMCT-N_i thermodynamic model based on the ion–molecule coexistence theory (IMCT) has the ability to simultaneously calculate the reaction abilities of simple and complex components in slag, and further calculate the phosphorus enrichment possibility of P_2O_5 containing solid solution. The essence of IMCT is the slag structure theory with all possible compounds including simple ions, simple molecules and complex molecules in the phase diagram as the structural units, and the mass action concentrations of structural units or ion couples in slag are quantitatively calculated using the mass action law to characterize the reaction capacity of the corresponding components.[48] Especially IMCT can directly calculate the reaction ability of calcium silicate and calcium phosphate in slag, which are the most relevant to the slag dephosphorization capacity. In addition, the empirical coefficient is more or less applied to the other eight activity prediction models. IMCT calculates the activity of slag components based on the mass conservation law and Gibbs free energy of reaction, and it does not need to introduce new coefficients. Based on the above reasons, IMCT is the thermodynamic model more suitable for evaluating the phosphorus enrichment capacity of slag.

Zhang[48] conducted systematic thermodynamic studies on the reaction ability of components in metallurgical slag based on IMCT. The mass action concentrations of the slag components can be in good agreement with the activities measured in the experiment under the studied slag compositions and temperature range. Yang *et al.*[60,61] studied the dephosphorization and desulfurization capacity of steelmaking slag based on IMCT, and they established thermodynamic models to predict the distribution ratio of phosphorus and sulfur between slag and molten steel. Li *et al.*[62] calculated the phosphorus enrichment degree of different P_2O_5 containing solid solutions in steelmaking slag based on IMCT, and discussed the phosphorus enrichment behavior of CaO–FeO–Fe_2O_3–SiO_2–MgO slag at 1450 °C to 1600 °C. Xie *et al.*[7] defined the phosphorus enrichment contribution ratio of calcium silicate in the slag based on IMCT, and studied the influence of basicity, m(FeO)/m(Fe_2O_3), FeO and P_2O_5 content on the phosphorus enrichment contribution ratio of four kinds of calcium silicate in multiphase slag at 1350 °C. In our previous work, the IMCT was used to quantitatively calculated the phosphorus enrichment contribution ratio of different calcium silicates in dephosphorization slag at different temperatures and basicities for the NDSP industrial experiments.[4,36] Further, we established prediction models of phosphorus distribution ratio and phosphate capacity in decarburization stage of NDSP,[63] and compared the average relative error and standard deviation of empirical models and IMCT model to evaluate the accuracy of IMCT model.[64] These results all show that IMCT is a reliable thermodynamic calculation method.

In the present work, the phosphorus enrichment capacity of four kinds of calcium silicate in multiphase dephosphorization slag under different process parameters was quantitatively calculated based on the laboratory high temperature experiments and IMCT. The innovation of this paper is summarized as the following three points: (I) Based on IMCT-N_i thermodynamic model, the influence of process parameters on the reaction ability of simple and complex components in CaO–SiO_2–FeO–MgO–MnO–P_2O_5–Al_2O_3 multiphase dephosphorization slag was calculated. The oxidation ability of dephosphorization slag under different process parameters was discussed, and the mathematical relationship between them was regressed. (II) The phosphorus enrichment contribution ratio of four kinds of calcium silicate and the phosphorus enrichment degree of P_2O_5 containing solid solution in multiphase dephosphorization slag under different process parameters were quantitatively clarified, and the correlation degree between phosphorus enrichment contribution ratio of calcium silicate and different process parameters is discussed. (III) The coefficient n of C_nS–C_3P in multiphase dephosphorization slag is estimated under different process parameters based on the experimental measurement results. The changing trends of phosphorus enrichment capacity of CS and C_2S in multiphase dephosphorization slag at different process parameters are mutually verified by IMCT and laboratory experiments.

II. LABORATORY HIGH TEMPERATURE EXPERIMENTS

In order to clarify the dephosphorization behavior of hot metal in dephosphorization stage of NDSP under complex conditions, a series of laboratory high temperature experiments under multi parameter conditions were carried out by simulating the experimental conditions of low temperature and low basicity in dephosphorization stage of NDSP. These research results can be found in our published literatures.[23,25,28–30] In the present work, the studied process parameters variables include slag basicity, temperature, Fe_2O_3 addition amount, initial P content of hot metal and reaction time.

The laboratory high temperature experiments are carried out with vacuum induction furnace and tube electric resistance furnace, as shown in Figs. 2(a) and (b). Figure 2(c) shows the schematic diagrams of hot metal sample and slag sample. The vacuum induction furnace is used to smelt the initial hot metal, and the tube electric resistance furnace is used for slag–hot metal dephosphorization reaction. The detailed process of sample preparation and experiment can be found in our previous papers.[23,25,28] The hot metal sample after dephosphorization is taken by a quartz tube with a length of 60 cm, a outer diameter of 14 mm and a wall thickness of 2 mm, as shown in Figure 2(c). The sample of dephosphorization slag will be adhered onto the wall

Table II. Activity Prediction Models of Slag Components

Activity Prediction Model	Scholar	Model Description	Calculation Applicability in Slag			Year	References
			Oxide	Silicate	P_2O_5 Containing Solid Solution		
Monte Carlo model	Borgianni *et al.*	thermodynamic and structural properties of silicate, aluminate and aluminosilicate are studied by Monte Carlo method	√	√	×	1977	[43]
Ionic Two-Sub-lattice Model	Hillert *et al.*	a new model to describe the change of thermodynamic properties when the melt gradually changes from a pure metal state to a fully ionized state by introducing neutral species and hypothetical vacancies with induced charges on the anion sublattice	×	×	×	1985	[44]
Associated Solution Model	Schmid *et al.*	based on the quasi-lattice theory, it is assumed that there are some atomic groups of fixed components in the phase. The solution can be treated to be composed of association complex and end group components. The interactions between components and between components and association complex conform to the regular solution model	√	×	×	1985	[45]
Ion–Molecular Coexistence theory	Zhang *et al.*	IMCT is the slag structure theory with all possible compounds including simple ions, simple molecules and complex molecules in the phase diagram as the structural units, and the mass action concentrations of structural units or ion couples in slag are quantitatively calculated using the mass action law to characterize the reaction capacity of the corresponding components	√	√	√	1990	[46–48]
Modified Quasi-chemical Model	Pelton *et al.*	Pelton *et al.* proposed a modified quasi-chemical solution model by modifying the classical quasi-chemical solution model. The specific correction is as follows: assuming that there is a maximum short-range ordered "pair" in the binary system, which means that anion and cation pairs can be freely combined. In view of the addition of the relationship of "pair", some changes are caused to the Gibbs free energy form of the system. The formula composed of substances defines new parameters to represent the change of Gibbs free energy when the maximum short-range ordered "pair" is formed. Finally, the binary system is extended to the multi-component system	√	×	×	1993	[49–52]

Table II. continued

Activity Prediction Model	Scholar	Model Description	Calculation Applicability in Slag: Oxide	Silicate	P_2O_5 Containing Solid Solution	Year	References
Regular Solution Model	Ban-Ya	in this model, it is assumed that different cations, such as Ca2+, Fe2+, Si4+ and Mg2+, are randomly distributed in the O2− matrix, and O2− is the common anion of various cations in the slag. The activity coefficient of oxide is calculated by the interaction energy between cations, and then its activity can be calculated	√	×	×	1993	[53]
Semiempirical Slag Model of Royal Institute of Technology	Seethara-man *et al.*	the model considers that the slag is completely ionic. The mixing of cations and anions is restricted to their respective subgroups, and complex ions are considered to be decomposed into simple entities. For example, $[SiO_4]^{4-}$ ion is considered to exist in the form of Si^{4+} and $4O^{2-}$ ion, and the influence of composite ion formation is considered to be part of the interaction between various simple ion species	√	×	×	1994	[54–56]
Molecular Interaction Volume Model	Tao *et al.*	based on lattice theory and free volume theory, the thermodynamic partition function of liquid and its mixture is derived using statistical thermodynamics, and the molecular interaction volume model is established	√	×	×	2006	[57, 58]
Cell Model	Zhang *et al.*	the model treats the melt as a mixture of cells formed among oxygen atoms and "cations". Model parameters to be determined are the cell formation energy and the cell interaction energy used in the expression of the free energy of mixing, while the cell formation energy and cell interaction energy can be functions of both temperature and composition	√	×	×	2007	[59]

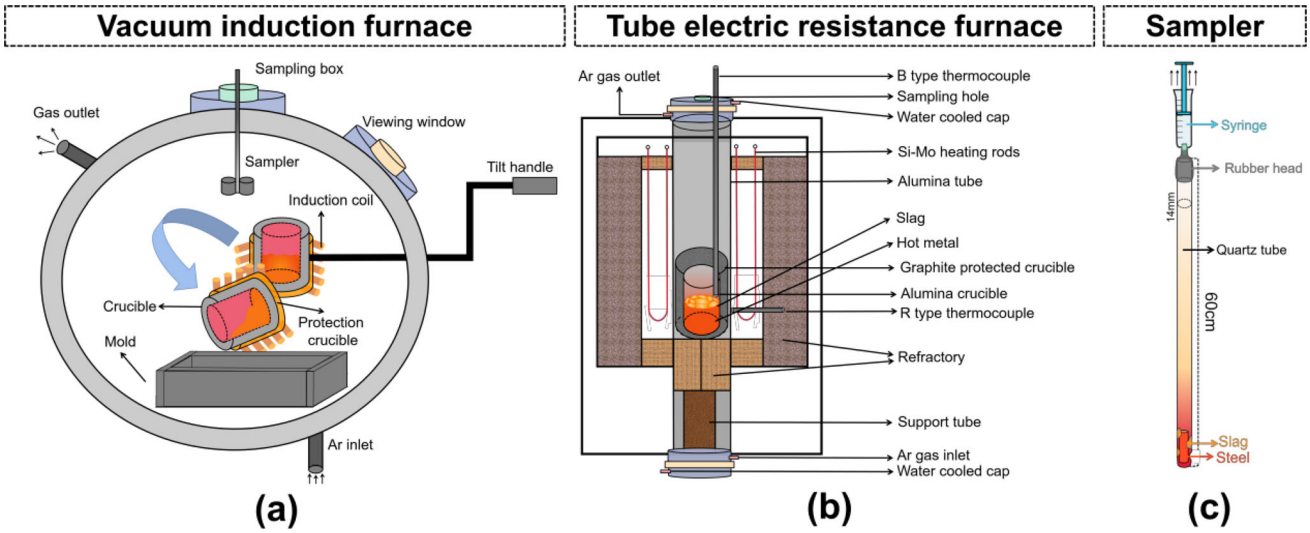

Fig. 2—Schematic diagrams of (*a*) vacuum induction furnace and (*b*) tube electric resistance furnace used in laboratory high temperature experiment, and (*c*) schematic diagrams of hot metal sample and slag sample.

of quartz tube, and we also used an iron bar with a length of 100 cm to stick the sample of dephosphorization slag. These samples are cooled in air and collected at room temperature.

The components of dephosphorization slag selected in the present work are $CaO–SiO_2–FeO–MgO–MnO–P_2O_5–Al_2O_3$, and the sum of the mass fractions of the seven components in the dephosphorization slag is supplemented to 100 according to the original proportion to ensure that these slag compositions are suitable for subsequent thermodynamic calculation. Table III lists the P contents of initial and finial hot metal, compositions and basicities of dephosphorization slag in laboratory experiment under different process conditions. The slag basicity, B, is calculated with Eq. [2].

$$B = \frac{(\text{pct CaO})}{(\text{pct SiO}_2)}. \quad [2]$$

Dephosphorization ratio η_P of hot metal and phosphorus distribution ratio L_P between slag and steel are the most intuitive indexes to express dephosphorization result of hot metal, and they can be calculated with Eqs. [3] and [4], respectively. $[\text{pct P}]_I$ and $[\text{pct P}]_E$ represent the initial and endpoint phosphorus contents of hot metal, respectively. Figures 3(a) through (e) show the effect of slag basicity, temperature, Fe_2O_3 addition amount, initial P content and time on dephosphorization ratio of hot metal and phosphorus distribution ratio between slag and hot metal.

$$\eta_P = \frac{[\text{pct P}]_I - [\text{pct P}]_E}{[\text{pct P}]_I} \times 100 \text{ pct}, \quad [3]$$

$$\log\ L_P = \log\left(\frac{(\text{pct P}_2\text{O}_5)}{[\text{pct P}]_E}\right). \quad [4]$$

According to Figures 3(a) through (e), with increasing slag basicity from 0.98 to 2.13, the η_P increases from 50.6 to 77.7 pct, and the L_P increases from 1.53 to 1.86. When the temperature is increased from 1300 °C to 1375 °C, the η_P increases from 17.9 to 73.2 pct, and the L_P increases from 1.10 to 1.79. However, with the temperature further increased to 1450 °C, the η_P decreases to 23.5 pct, and the L_P decreases to 1.23. With increasing Fe_2O_3 addition amount from 5 to 30 g gradually, the η_P and the L_P increase from − 3.34 to 81.3 pct and from 1.03 to 2.34, respectively. Taking the initial P content of hot metal as the research variable, the η_P and L_P both increase first and then decrease with increasing initial P content of hot metal. When the initial phosphorus content is 0.173 pct, the η_P and L_P have the highest values, which are 83.2 pct and 2.21, respectively. With the extension of dephosphorization reaction time from 3 to 15 minutes, the η_P increases from 15.7 to 83.2 pct, and the L_P increases from 1.33 to 2.21. When the reaction time further extends to 18 minutes, the η_P and the L_P are slightly decreased to 80.2 pct and 1.96, which are caused by the rephosphorization of hot metal. Among the five process parameters that affect the dephosphorization of hot metal, the Fe_2O_3 addition amount has the largest change range of 84.6 pct on dephosphorization ratio of hot metal, while the initial P content of hot metal has the smallest change range of 16.6 pct on the dephosphorization ratio of hot metal.

The horizontal section containing $C_2S–C_3P$ at 1350 °C and the liquidus projection of $CaO–SiO_2–FeO–(5$ mass pct MgO–5 mass pct MnO–4 mass pct $P_2O_5)$ at 1300 °C to 1450 °C were calculated using the Phase diagram of FactSage 8.1 thermodynamic software. Figure 4(a) shows the dephosphorization slag compositions of different process parameters in $CaO–SiO_2–FeO–(5$ mass pct MgO–5 mass pct MnO–4 mass pct $P_2O_5)$ pseudo ternary phase diagram at 1300 °C to 1450 °C. Figures 4(b) through (d) show the change path of dephosphorization slag compositions in

Table III. P Contents in Initial and Final Hot Metal, Compositions and Basicities of Dephosphorization Slag in Laboratory Experiment Under Different Process Parameters

Process Parameters			Collection of Experimental Results											
			P Content in Hot Metal (Pct)		Compositions of Dephosphorization Slag (Pct)									References
Variables	No	Variable Value	$[P]_I$	$[P]_E$	CaO	SiO_2	FeO	MgO	MnO	P_2O_5	Al_2O_3	B (—)	T (°C)	
Slag Basicity (—)	1-1	0.98	0.253	0.125	21.04	21.54	33.33	4.04	5.22	4.24	10.59	0.98	1350	[29]
	1-2	1.17	0.282	0.104	23.04	19.60	34.46	3.31	4.53	4.11	10.95	1.17	1350	
	1-3	1.31	0.286	0.092	26.07	19.95	29.38	3.29	4.46	4.71	12.15	1.31	1350	
	1-4	1.55	0.311	0.095	31.38	20.22	26.55	3.20	3.88	4.36	10.41	1.55	1350	
	1-5	1.86	0.304	0.080	34.07	18.29	27.24	3.28	3.46	4.82	8.84	1.86	1350	
	1-6	2.13	0.273	0.061	33.57	15.78	29.55	3.00	3.30	4.41	10.39	2.13	1350	
Temperature (°C)	2-1	1300	0.201	0.165	28.37	12.78	46.36	5.41	3.49	2.09	1.49	2.22	1300	[23]
	2-2	1325	0.209	0.079	30.50	15.41	37.43	5.74	3.66	3.22	4.04	1.97	1325	
	2-3	1350	0.242	0.069	29.45	15.47	35.67	5.36	4.10	4.01	5.94	1.91	1350	
	2-4	1375	0.246	0.066	33.23	16.46	29.76	6.20	3.85	4.10	6.39	2.03	1375	
	2-5	1400	0.216	0.091	32.37	17.35	24.76	5.92	4.28	4.31	11.00	1.86	1400	
	2-6	1425	0.238	0.124	29.01	15.41	27.88	5.17	3.09	2.65	16.79	1.88	1425	
	2-7	1450	0.204	0.156	28.41	15.42	23.62	4.83	3.45	2.63	21.65	1.85	1450	
Fe_2O_3 Addition Amount (g)	3-1	5	0.265	0.274	37.64	22.31	20.71	6.94	4.69	2.91	4.80	1.69	1350	[25]
	3-2	10	0.261	0.251	32.26	20.33	28.02	5.73	4.50	2.91	6.24	1.59	1350	
	30-3	12.5	0.271	0.163	31.62	20.77	21.79	5.29	5.96	5.01	9.57	1.52	1350	
	3-4	15	0.271	0.112	30.11	19.97	26.03	5.38	5.57	5.52	7.41	1.51	1350	
	3-5	20	0.263	0.080	29.64	20.57	23.19	4.97	5.61	5.80	10.22	1.44	1350	
	3-6	25	0.269	0.050	24.98	17.41	34.30	4.71	5.08	5.76	7.76	1.44	1350	
	3-7	30	0.27	0.045	26.13	18.17	29.91	5.05	5.42	6.26	9.06	1.44	1350	
Initial P Content (Pct)	4-1	0.057	0.057	0.019	22.18	14.78	43.47	3.68	4.66	2.39	8.85	1.50	1350	[28]
	4-2	0.098	0.098	0.029	21.44	14.33	43.68	3.84	4.77	3.03	8.93	1.50	1350	
	4-3	0.173	0.173	0.029	24.48	16.59	36.12	4.47	5.39	4.69	8.25	1.48	1350	
	4-4	0.249	0.249	0.044	24.17	16.15	36.26	4.32	5.42	5.44	8.23	1.49	1350	
	4-5	0.292	0.292	0.063	23.54	16.77	35.87	4.08	5.39	5.85	8.49	1.40	1350	
Time (Min)	5-1	3	0.159	0.134	23.39	14.43	48.99	3.67	4.27	2.85	2.40	1.62	1350	[30]
	5-2	6	0.251	0.086	22.57	15.01	47.87	3.52	4.63	3.40	3.00	1.50	1350	
	5-3	9	0.195	0.058	23.79	16.89	41.21	3.62	5.18	4.21	5.10	1.41	1350	
	5-4	12	0.209	0.042	25.05	18.74	35.15	4.11	4.80	4.81	7.36	1.34	1350	
	5-5	15	0.173	0.029	24.33	16.49	36.50	4.44	5.36	4.67	8.21	1.48	1350	
	5-6	18	0.248	0.049	24.00	18.17	35.94	3.98	4.71	4.52	8.68	1.32	1350	

$CaO–SiO_2–FeO–$(5 mass pct MgO–5 mass pct MnO–4 mass pct P_2O_5) pseudo ternary phase diagram under different basicities, temperatures, Fe_2O_3 addition amounts, initial P contents and times, respectively, whose change directions are described with the dotted arrow.

Combined with Figures 4(a) through (d), it can be seen that, within the temperature range of dephosphorization stage of NDSP, dephosphorization slags exist in the two phase state of solid–liquid coexistence, being almost all located in the area containing $C_2S–C_3P$ solid solution. It is worth noting that the composition point of dephosphorization slag with basicity lower than 1.17 is not located in the area containing $C_2S–C_3P$. According to our previous mineral phase analysis of dephosphorization slag,[4] this is due to the fact that massive P-rich phase cannot be effectively formed in the dephosphorization slag under low basicity conditions. Multiphase dephosphorization slag usually forms P_2O_5 containing solid solution in the dephosphorization stage of NDSP, and it contains part of the liquid phase to promote mass transfer, which makes the multiphase dephosphorization slag have better phosphorus enrichment capacity. The increase of slag basicity will promote the slag composition point to move to the CaO angle, and the increase of Fe_2O_3 addition amount will promote the slag composition point to move to the FeO angle. The increases of temperature, initial P content of hot metal and time will promote the slag composition point to move towards the lower part of the $CaO–SiO_2–FeO$ pseudo ternary phase diagram, which is caused by the decrease of FeO content in multiphase dephosphorization slag.

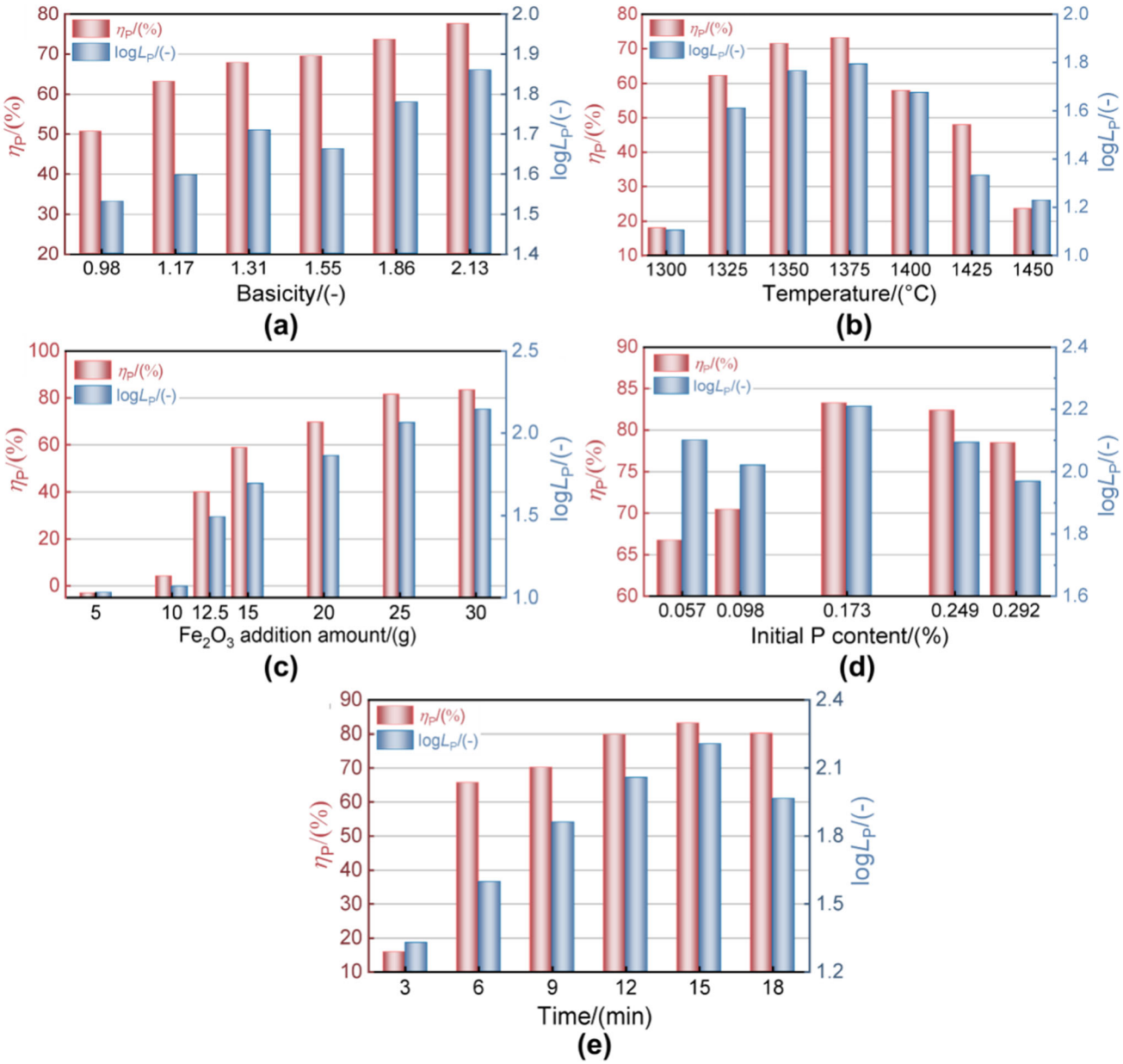

Fig. 3—Effect of (*a*) slag basicity, (*b*) temperature, (*c*) Fe_2O_3 addition amount, (*d*) initial P content and (*e*) time on dephosphorization ratio of hot metal and phosphorus distribution ratio between slag and hot metal.

III. RESULTS AND DISCUSSION

A. *Effect of Process Parameters on Mass Action Concentrations N_i of Structural Units in $CaO–SiO_2–FeO–MgO–MnO–P_2O_5–Al_2O_3$ Multiphase Dephosphorization Slag*

According to the established IMCT-N_i thermodynamic model,[4] the mass action concentrations of structural units in $CaO–SiO_2–FeO–MgO–MnO–P_2O_5–Al_2O_3$ multiphase dephosphorization slag under different process parameters are calculated quantitatively. The calculation formulas of mass action concentration of structural unit i and ion couples (Me^{2+} + O^{2-}) in slag are expressed as Eqs. [5] and [6].[4,58,63] N_i is defined as the ratio of equilibrium mole number of structural unit i or ion couples to the total equilibrium mole numbers $\sum N_i$ of all structural units in slag with a fixed amount. Figure 5 shows the effect of process parameters on mass action concentrations of simple components of CaO, SiO_2, FeO and P_2O_5 in multiphase dephosphorization slag.

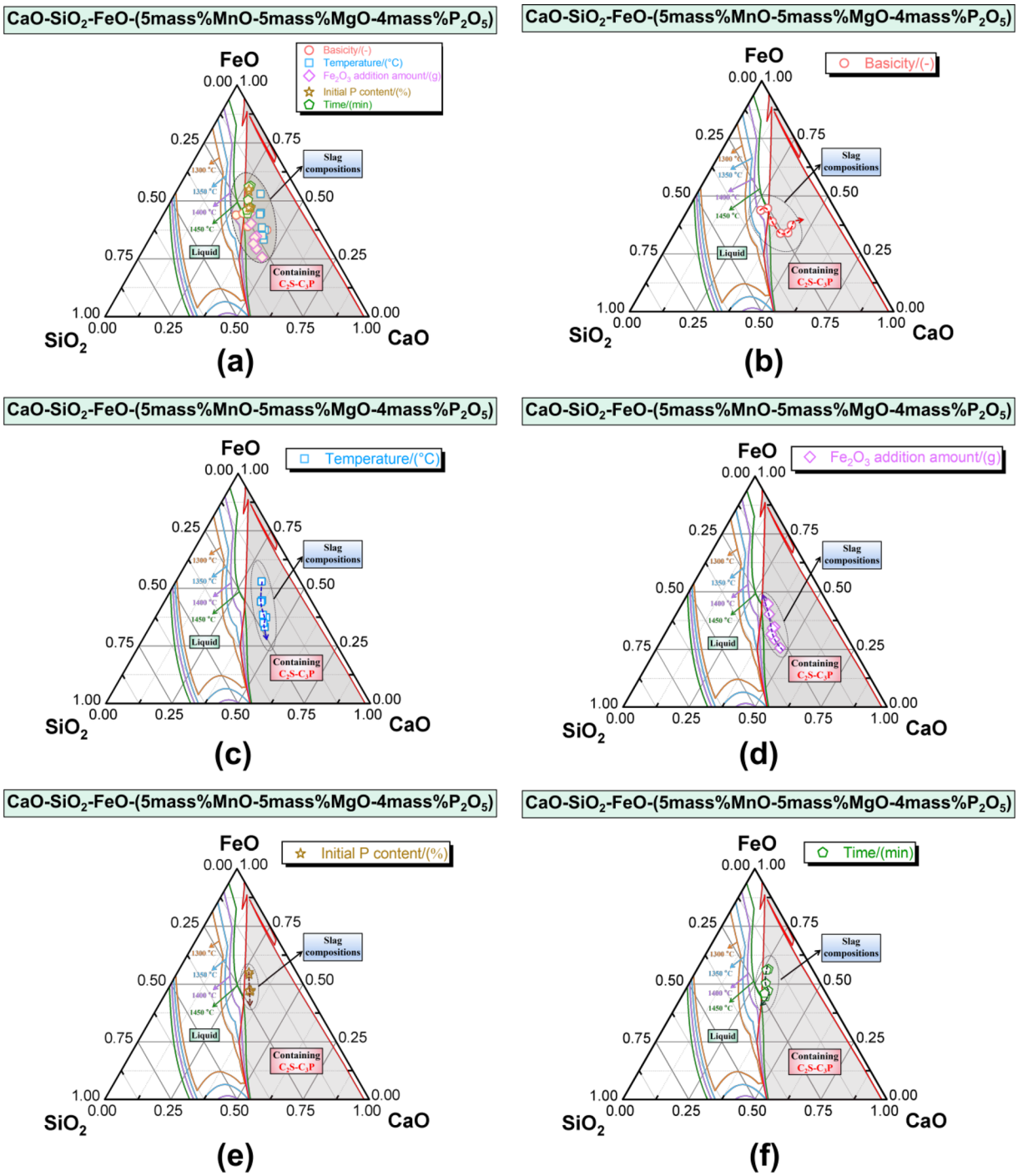

Fig. 4—Dephosphorization slag compositions of different process parameters in CaO–SiO_2–FeO–(5 mass pct MgO–5 mass pct MnO–4 mass pct P_2O_5) pseudo ternary phase diagram at 1300 °C to 1450 °C; change path of dephosphorization slag compositions in CaO–SiO_2–FeO–(5 mass pct MgO–5 mass pct MnO–4 mass pct P_2O_5) pseudo ternary phase diagram under different (*b*) basicities, (*c*) temperatures, (*d*) Fe_2O_3 addition amounts, (*e*) initial P contents and (*f*) times.

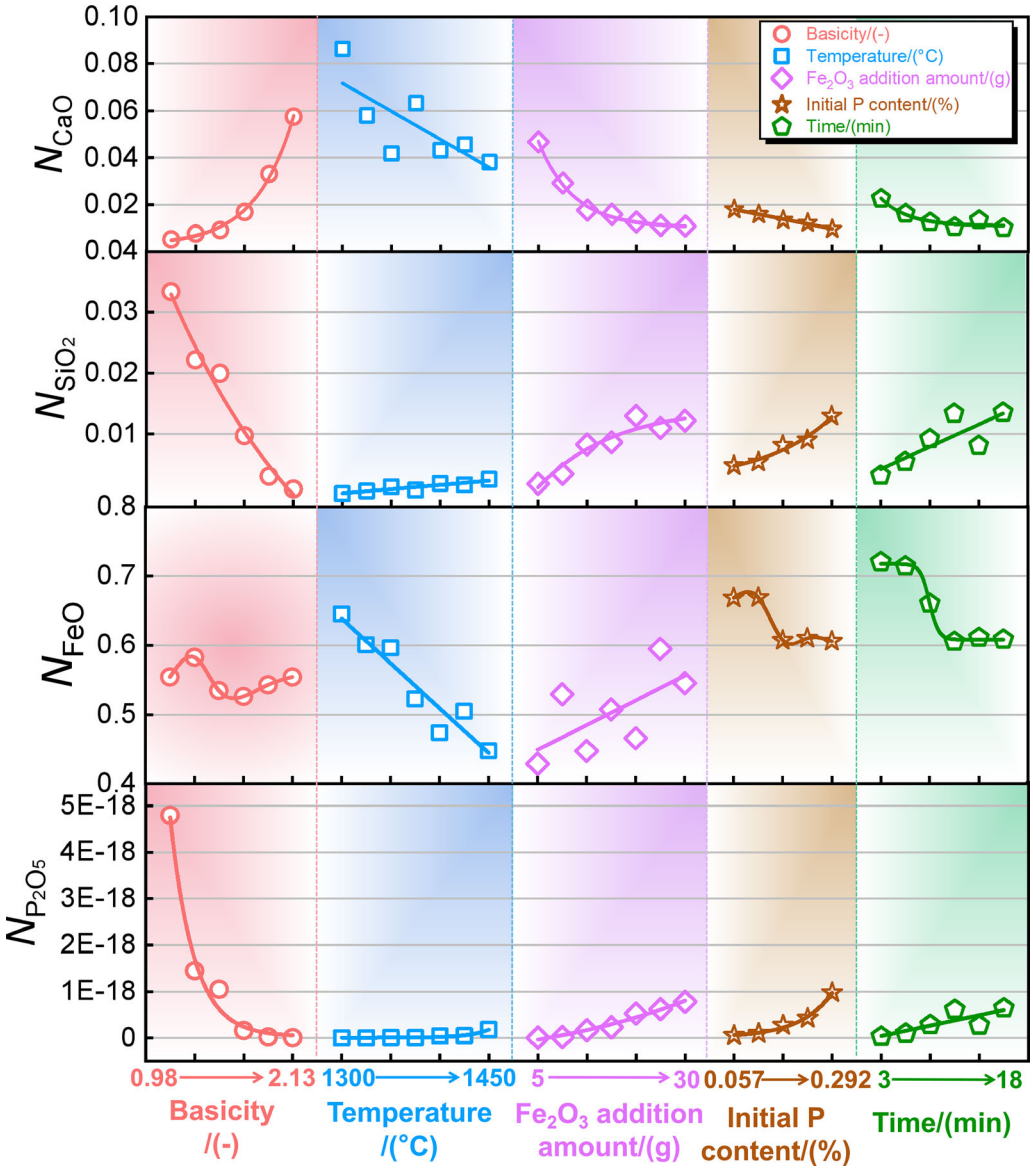

Fig. 5—Effect of process parameters on mass action concentrations of simple components of CaO, SiO_2, FeO and P_2O_5 in multiphase dephosphorization slag.

$$N_i = \frac{n_i}{\sum n_i}\ (-), \qquad [5]$$

$$N_{\mathrm{MeO}} = N_{\mathrm{Me^{2+},\,MeO}} + N_{\mathrm{O^{2-},\,MeO}} = \frac{n_{\mathrm{Me^{2+},\,MeO}} + n_{\mathrm{O^{2-},\,MeO}}}{\sum n_i} = \frac{2n_{\mathrm{MeO}}}{\sum n_i}. \qquad [6]$$

It can be seen from Figure 5 that with increasing slag basicity from 0.98 to 2.13, N_{CaO} increases exponentially, $N_{\mathrm{SiO_2}}$ and $N_{\mathrm{P_2O_5}}$ decreases exponentially, and N_{FeO} does not change significantly. The increase of the slag basicity means that the increase of CaO/SiO_2 ratio in the slag, which leads to the enhancement of CaO reaction ability and the reduction of SiO_2 reaction ability. The increase of slag basicity has no obvious effect on FeO reaction ability. The increase of temperature leads to linear decrease of N_{CaO} and N_{FeO}, respectively, while $N_{\mathrm{SiO_2}}$ and $N_{\mathrm{P_2O_5}}$ increase slightly. With increasing temperature, the slag will melt continuously, and the contents of CaO and

FeO that can be consumed in dephosphorization reaction increases gradually, leading to the reduction of N_{CaO} and N_{FeO}. With increasing Fe_2O_3 addition amount from 5 to 30 g, N_{FeO}, $N_{P_2O_5}$ and N_{SiO_2} show an overall increase trend, while N_{CaO} decreases exponentially. These results can be explained that the increase of iron oxide content in slag reduces the content of CaO, which decreases N_{CaO}. The increase of FeO content in the slag can effectively improve the phosphorus enrichment capacity of the dephosphorization slag, which increases $N_{P_2O_5}$.

When the initial P content of hot metal increases from 0.057 to 0.292 pct, $N_{P_2O_5}$ and N_{SiO_2} increase exponentially, respectively, N_{CaO} decreases linearly and N_{FeO} gradually decreases to a stable value. The increase of initial P content of hot metal enhances the possibility that free phosphorus in hot metal is enriched by slag, which increases $N_{P_2O_5}$. FeO is gradually consumed largely with the increase of initial P content of hot metal, which can be indicated by the change trend of N_{FeO}. With the extension of reaction time, N_{CaO} decreases exponentially, N_{FeO} decreases rapidly in the first ten minutes of experiment, and then stabilized at a constant level. N_{SiO_2} and $N_{P_2O_5}$ show an overall increase trend. The dephosphorization reaction of hot metal gradually reached equilibrium with the extension of time, and N_{FeO} continuously decreases until it stabilized to a constant value. The continuous dephosphorization reaction leads to the decrease of slag basicity, which decreases N_{CaO} and increases N_{SiO_2}. The reaction time is long enough to enable the phosphorus to be fully enriched by slag and stably removed from hot metal, and the details can refer to our previous work,[30] so $N_{P_2O_5}$ increases.

The change of reaction ability of complex components in multiphase dephosphorization slag under different process parameters is further studied. Figures 6(a) through (e) is the effect of process parameters, including basicity, temperature, Fe_2O_3 addition amount, initial P content and time on mass action concentrations of calcium silicates and calcium phosphates in multiphase dephosphorization slag. Table IV summarizes the change trend of mass action concentrations of calcium silicates and calcium phosphates in multiphase dephosphorization slag under different process parameters. Combined Figure 6 with Table IV, N_{CS} and N_{C_2S} are 1 to 2 orders of magnitude higher than N_{C_3S} and $N_{C_3S_2}$, N_{C_3P} are 2 to 3 orders of magnitude higher than N_{C_2P} and N_{C_4P}. Therefore, the reaction ability of CS, C_2S, C_3P and the P_2O_5 containing solid solution need to be focused on.

With increasing slag basicity from 0.98 to 2.13, the mass fraction of C_2S generated in multiphase dephosphorization slag gradually increases, which causes N_{C_2S} increase and N_{CS} decrease accordingly. The increase of slag basicity enhances the amount of free $(Ca^{2+} + O^{2-})$ in the slag, which is conducive to the formation of calcium phosphate with high proportion of CaO, so both N_{C_3P} and N_{C_4P} increase. With increasing temperature in the range of 1300 °C to 1400 °C, N_{CS}, N_{C_2S}, N_{C_2P}, N_{C_3P} and N_{C_4P} all increase, which is caused by the gradual melting of dephosphorization slag. When the temperature exceeds 1400 °C, the dephosphorization ratio of hot metal and the basicity of slag are decreased with increasing temperature, and the N_{C_2S}, N_{C_3P} and N_{C_4P} with high CaO content are decreased reasonably. With increasing Fe_2O_3 addition amount from 5 to 30 g, N_{CS} first increases and then decreases, and N_{C_2S} gradually decreases. The reaction ability of calcium silicate in the slag tends to weaken as a whole, which is caused by the increase of iron oxide content in the slag. The addition of iron oxide improves the dephosphorization capacity of slag, so N_{C_2P} and N_{C_3P} both can be increased. However, the C_4P with high CaO content is difficult to form because the content of CaO in the slag continuously decreases, so N_{C_4P} decreases.

With increasing initial P content ranging from 0.057 to 0.292 pct in hot metal, the reaction ability of calcium phosphate in the slag has an overall increasing trend, and N_{C_2P}, N_{C_3P} and N_{C_4P} all increase in varying degrees. N_{CS} increases slightly and N_{C_2S} decreases slightly. It can be seen that the initial P content of hot metal has no obvious effect on calcium silicate reaction ability in multiphase dephosphorization slag. With the extension of dephosphorization reaction time from 3 to 18 minutes, the slag basicity gradually decreases, leading to an increase in N_{CS} and a decrease in N_{C_2S}. The reaction ability of calcium phosphate in the slag increases as a whole with the extension of time. When the reaction time exceeds 12 minutes, N_{C_3P} slightly decreases. The reason is reasonably considered that the content of P_2O_5 in the slag is decreased due to the rephosphorization of hot metal, which leads to the reduction of calcium phosphate reaction ability.

B. *Analysis of Oxidation Capacity of Multiphase Dephosphorization Slag Under Different Process Parameters Based on IMCT*

The reaction ability of iron oxide in slag is a key index to characterize the oxidizability of slag. Figure 7 illustrates the effect of mass fraction of FeO on N_{FeO} under different process parameters.

With increasing FeO content in multiphase dephosphorization slag, N_{FeO} increases exponentially, and the relationship between them is not affected by process parameters. The mathematical relationship between the mass fraction of FeO and its mass action concentration N_{FeO} is further discussed through juxtaposition fitting data, as shown in Eq. [7]. The fitting coefficient, r^2, of Eq. [7] is as high as 0.96, which indicates that the reaction ability of FeO is mainly related to the mass fraction of FeO in multiphase dephosphorization slag.

$$N_{FeO} = -0.901 \times \exp\left(-\frac{(\text{mass pct FeO})}{37.959}\right) + 0.953, \quad r^2 = 0.96. \qquad [7]$$

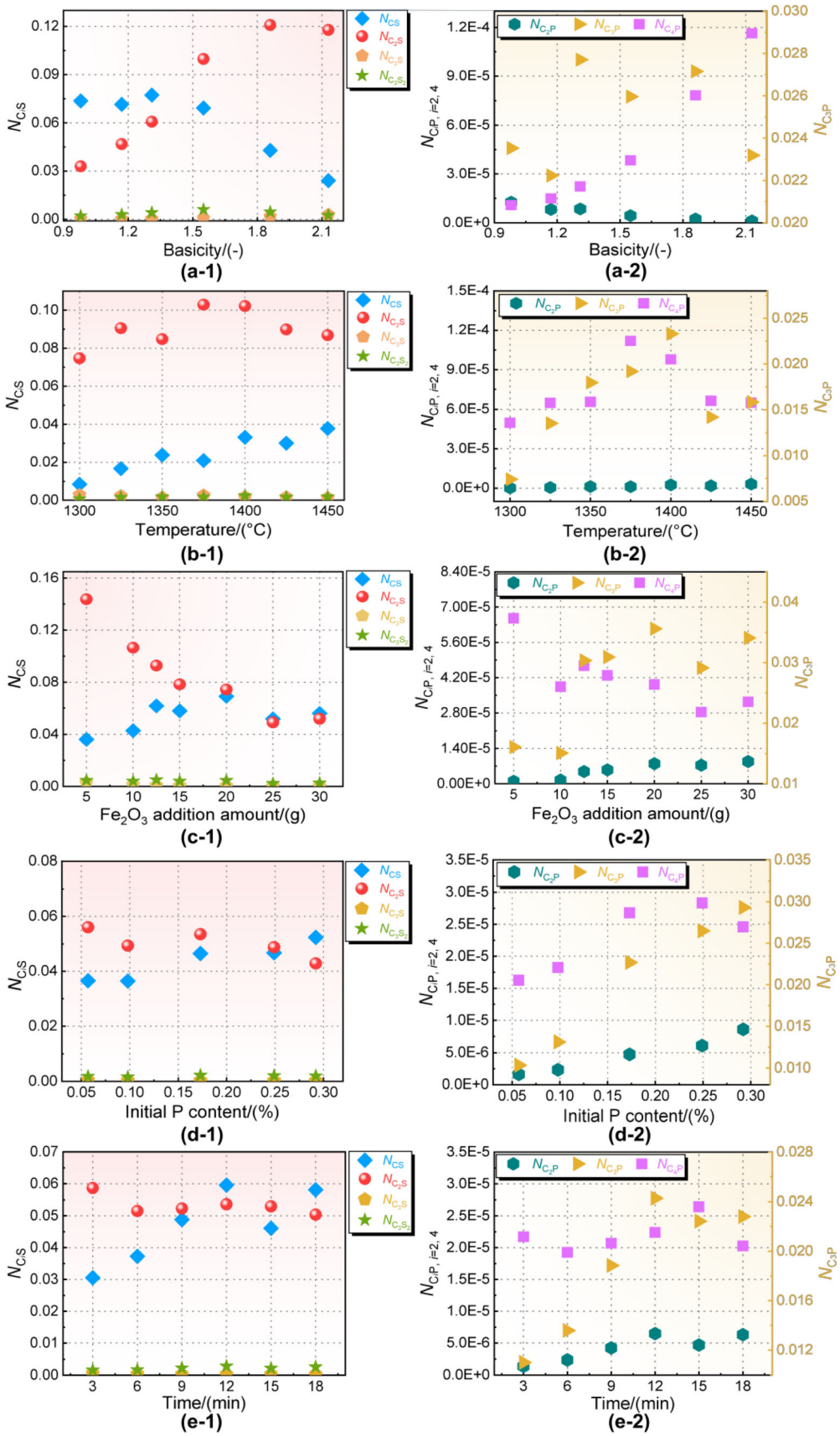

Fig. 6—Effect of process parameters of (*a*) basicity, (*b*) temperature, (*c*) Fe_2O_3 addition amount, (*d*) initial P content and (*e*) time on mass action concentrations of calcium silicates and calcium phosphates in multiphase dephosphorization slag.

Table IV. Change Trend of Mass Action Concentrations of Calcium Silicates and Calcium Phosphates in Multiphase Dephosphorization Slag Under Different Process Parameters

Components		Slag Basicity (—)	Temperature (°C)	Fe_2O_3 Addition Amount (g)	Initial P Content (Pct)	Time (Min)
Calcium Silicate	CS	→	↑	(5 to 20)↑, (20 to 30)↓	↑	↑
	C_2S	←	(1300 to 1400)↑, (1400 to 1450)↓	→	→	→
	C_3S	←	→	→	→	→
	C_3S_2	(0.98 to 1.55)↑, (1.55 to 2.13)↓	↑	→	(0.057 to 0.173)↑, (0.173 to 0.292)↓	↑
	C_2P	→	←	←	←	←
Calcium Phosphate	C_3P	(0.98 to 1.86)↑, (1.86 to 2.13)↓	(1300 to 1400)↑, (1400 to 1450)↓	↑	↑	(3 to 12)↑, (12 to 18)↓
	C_4P	←	(1300 to 1375)↑, (1375 to 1450)↓	→	(0.057 to 0.249)↑, (0.249 to 0.292)↓	(3 to 15)↑, (15 to 18)↓

Fig. 7—Effect of mass fraction of FeO on N_{FeO} under different process parameters.

Based on the classic hypothesis of IMCT, the basic oxides CaO ($Ca^{2+} + O^{2-}$), MnO ($Mn^{2+} + O^{2-}$), FeO ($Fe^{2+} + O^{2-}$) and MgO ($Mg^{2+} + O^{2-}$) exist in multiphase dephosphorization slag in the form of ion couples, and they can all produce free O^{2-}. While acidic oxides P_2O_5 and SiO_2 exist in the multiphase dephosphorization slag in molecular form and cannot produce free O^{2-}. Al_2O_3 is considered as amphoteric oxide in the present slag components, which is not considered in the process of calculating slag oxidizability. According to the above analysis, the ratio of mass action concentration of basic oxide to acid oxide can reasonably represent the reaction capacity of free O^{2-} in slag, and further characterize the oxidation capacity of multiphase dephosphorization slag, as shown in Eq. [8].

$$\frac{N_{\text{basic oxide}}}{N_{\text{acidic oxide}}} = \frac{(N_{CaO} + N_{FeO} + N_{MnO} + N_{MgO})}{(N_{SiO_2} + N_{P_2O_5})}, \ (-). \quad [8]$$

Figures 8(a) through (e) show the effect of process parameters, including basicity, temperature, Fe_2O_3 addition amount, initial P content and time on the ratio of mass action concentration of basic oxide to acidic oxide, and Figure 8(f) shows the relationship between the ratio of mass percentage of basic oxide to acidic oxide and its the ratio of mass action concentration. It can be seen from Figures 8(a) through (e) that the increase of slag basicity makes the reaction capacity of free O^{2-} in slag significantly enhanced, which is due to the increase of ($Ca^{2+} + O^{2-}$) content in the slag. The increase of process parameters, such as temperature, Fe_2O_3 addition amount, initial P content and time, will reduce the reaction capacity of free O^{2-} in slag varying degrees. The reason can be reasonably explained as that under the influence of these process parameters, the basicity of multiphase dephosphorization slag and the total content of basic oxides are reduced in varying degrees, which will reduce the O^{2-} produced by dynamic equilibrium in the slag. It is worth noting that in Figure 8(c), even if the Fe_2O_3 addition amount

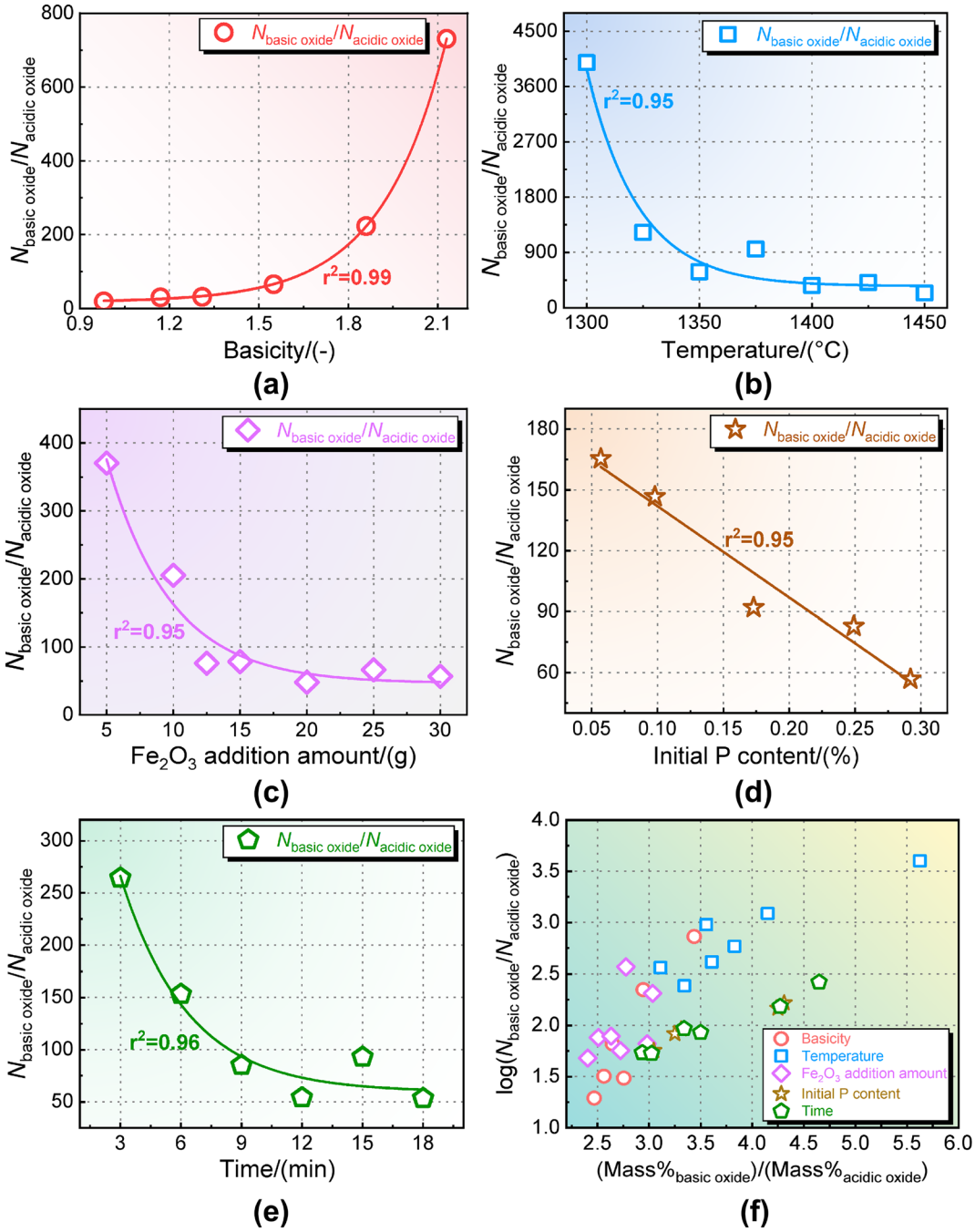

Fig. 8—Effect of process parameters of (*a*) basicity, (*b*) temperature, (*c*) Fe_2O_3 addition amount, (*d*) initial P content and (*e*) time on the ratio of mass action concentration of basic oxide to acidic oxide, and (*f*) relationship between the ratio of mass percentage of basic oxide to acidic oxide and its the ratio of mass action concentration.

gradually increases, the ratio of the mass action concentration of basic oxides to acid oxides still decreases exponentially, because the CaO content in the slag decreases significantly with the increase of FeO content, which makes the reaction capacity of free O^{2-} in slag decrease as a whole.

$$\frac{N_{\text{basic oxide}}}{N_{\text{acidic oxide}}} = 0.038\exp\left(\frac{\text{Basicity}}{0.216}\right) + 17.857, r^2 = 0.99, \quad [9-1]$$

$$\frac{N_{\text{basic oxide}}}{N_{\text{acidic oxide}}} = 2.001 \exp\left(\frac{\text{Temperature}}{-22.808}\right) + 354.039, \quad r^2 = 0.95, \qquad [9-2]$$

$$\frac{N_{\text{basic oxide}}}{N_{\text{acidic oxide}}} = 934.84 \exp\left(\frac{\text{Fe}_2\text{O}_3 \text{ addition amount}}{-4.797}\right) + 46.336, \quad r^2 = 0.95, \qquad [9-3]$$

$$\frac{N_{\text{basic oxide}}}{N_{\text{acidic oxide}}} = -450.604(\text{Initial P content}) + 187.055, \quad r^2 = 0.95, \qquad [9-4]$$

$$\frac{N_{\text{basic oxide}}}{N_{\text{acidic oxide}}} = 509.661 \exp\left(\frac{\text{Time}}{-3.326}\right) + 59.437, \quad r^2 = 0.96. \qquad [9-5]$$

There is the obvious mathematical relationships between the different process parameters and the reaction capacity of free O^{2-} in the slag, as shown in Eqs. (9-1) through [9-5], and the regression coefficients between them are greater than 0.94. Figure 8(f) shows that the ratio of the mass percentage of basic oxides to acidic oxides is positively related to its mass action concentration ratio. Therefore, the oxidation capacity of multiphase dephosphorization slag can be improved by increasing the overall content of basic oxides.

C. *Change of Phosphorus Enrichment Contribution Ratio of Four Kinds of Calcium Silicate in Multiphase Dephosphorization Slag Under Different Process Parameters*

The slag basicity can obviously affect the type of calcium silicate generated in the multiphase dephosphorization slag, and further effect the phosphorus enrichment capacity of the multiphase dephosphorization slag. Figure 9 demonstrates the effect of the ratio of CaO/SiO_2 on its the ratio of mass action concentration under different process parameters.

With increasing slag basicity, $\log(N_{CaO}/N_{SiO_2})$ increases exponentially. Equation [10] regresses the mathematical relationship between slag basicity and $\log(N_{CaO}/N_{SiO_2})$, and the fitting coefficient, r^2, between them is 0.93, which indicates that changes in process parameters will not significantly influence their relationship. Among the five process parameters currently studied, the effect of temperature on $\log(N_{CaO}/N_{SiO_2})$ is the most obvious, as shown in blue square in Figure 9.

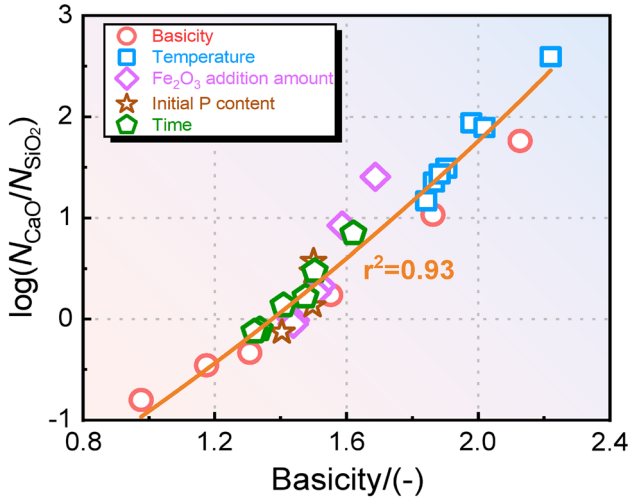

Fig. 9—Effect of the ratio of CaO/SiO_2 on its the ratio of mass action concentration under different process parameters.

$$\log(N_{CaO}/N_{SiO_2}) = 6.208 \times \exp\left(\frac{B}{3.554}\right) - 9.138. \qquad [10]$$

The phosphorus enrichment capacities of four kinds of calcium silicate CS, C_2S, C_3S, C_3S_2 in multiphase dephosphorization slag are further quantitatively calculated based on the phosphorus enrichment contribution ratio R_{Ci} of calcium silicate defined by IMCT. Taking C_2S as an example, R_{C_2S} can be calculated by Eq. [11], and the detailed derivation process can be found in our previous paper,[4] in which N_{Ci-Pj} is the phosphorus enrichment possibility of P_2O_5 containing solid solution, R_{Ci-Pj} is the phosphorus enrichment degree of P_2O_5 containing solid solution, and M_i is the relative molecular mass of component i.

$$R_{C_2S} = R_{C_2S-C_2P} + R_{C_2S-C_3P} + \cdots + R_{C_2S-Mg_2P} + R_{C_2S-Mg_3P} = \frac{\sum_{i=2}^{j=1-8} \left(N_{C_2S-Pj} \frac{M_{P_2O_5}}{M_{C_2S-Pj}}\right)}{\sum_{\substack{i=1-3 \\ j=1-8}} \left(N_{Ci-Pj} \frac{M_{P_2O_5}}{M_{Ci-Pj}}\right)}. \qquad [11]$$

Figures 10(a) through (e) shows the variation of phosphorus enrichment contribution ratio of four kinds of calcium silicate in multiphase dephosphorization slag under different basicities, temperatures, Fe_2O_3 addition amounts, initial P contents and times. The three-dimensional bar chart diagram on the left side of Figure 10 presents the comprehensive influence of process parameters and dephosphorization ratio of hot metal on the phosphorus enrichment contribution ratio of calcium silicate, and the two-dimensional line diagram on the right side of Figure 10 illustrates the mathematical relationship between different process parameters and the phosphorus enrichment contribution ratio of four kinds of calcium silicate.

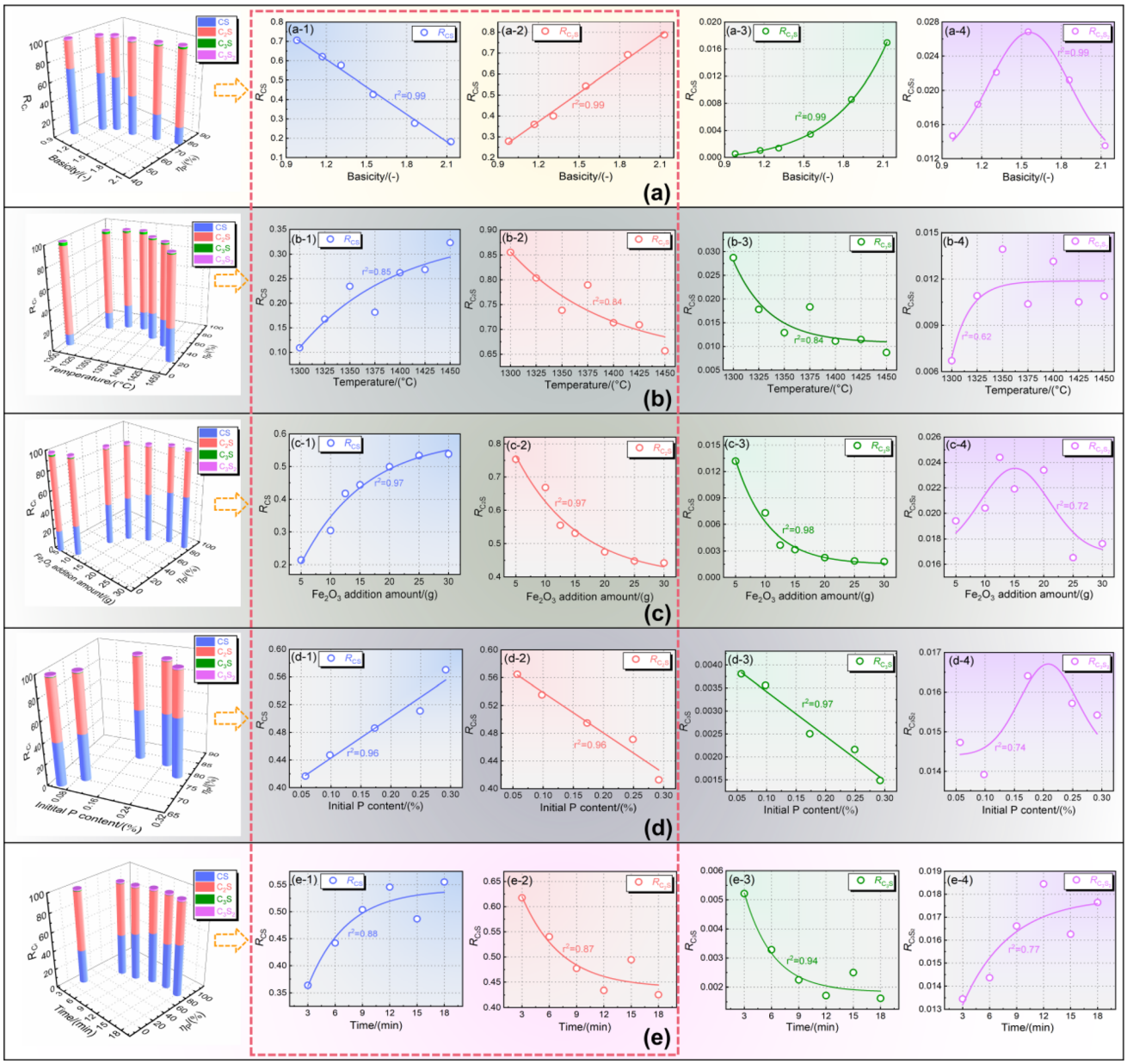

Fig. 10—Variation of phosphorus enrichment contribution ratio of four kinds of calcium silicate in multiphase dephosphorization slag under different (*a*) basicities, (*b*) temperatures, (*c*) Fe_2O_3 addition amounts, (*d*) initial P contents and (*e*) times.

It can be seen from Figures 10(a) through (e) that the sum of the phosphorus enrichment contribution ratios of CS and C_2S accounts for more than 95 pct of the total phosphorus enrichment contribution ratios of four kinds of calcium silicate, which indicates that the CS and C_2S are the calcium silicate that play the main role of enriching phosphorus in multiphase dephosphorization slag. Further, the change rule of R_{CS} and R_{C_2S} in multiphase dephosphorization slag are discussed emphatically. Figure 10(a) shows that with the slag basicity increasing from 0.98 to 2.13, R_{CS} decreases linearly from 0.71 to 0.18, while R_{C_2S} increases linearly from 0.28 to 0.79. The increase of slag basicity significantly enhances the generation content of C_2S in multiphase dephosphorization slag, the phosphorus enrichment capacity of C_2S is improved and the dephosphorization ratio of hot metal increases to 77.7 pct when the slag basicity is 2.13. According to Figure 10(b), with increasing temperature from 1300 °C to 1450 °C, R_{CS} increases exponentially from 0.11 to 0.32, while R_{C_2S} decreases exponentially from 0.86 to 0.66. These results can be reasonably explained that CaO in multiphase dephosphorization slag gradually melt with increasing temperature, which makes the proportion of CS generation in slag gradually increase and the proportion of C_2S generation gradually decrease. Therefore, the phosphorus enrichment capacity of CS in multiphase dephosphorization gradually increases, while C_2S is the opposite. Combined with Figure 10(b) and Table III, the slag basicity is always

Table V. Change Trend of Phosphorus Enrichment Contribution Ratio of Four Kinds of Calcium Silicate in Multiphase Dephosphorization Slag Under Different Process Parameters

R_i	Slag Basicity (—)	Temperature (°C)	Fe_2O_3 Addition Amount (g)	Initial P Content (Pct)	Time (Min)
CS	↓	↑	↑	↑	↑
C_2S	↑	↓	↓	↓	↓
C_3S	↑	↓	↓	↓	↓
C_3S_2	(0.98 to 1.55)↑, (1.55 to 2.13)↓	↑	(5 to 15)↑, (15 to 30)↓	(0.057 to 0.173)↑, (0.173 to 0.292)↓	↑

above 1.85 in the experiment with temperature as the variable, so the phosphorus enrichment capacity of C_2S in multiphase dephosphorization slag is always stronger than that of CS. When the Fe_2O_3 addition amount increases from 5 to 30 g, R_{CS} increases exponentially from 0.21 to 0.54, and R_{C2S} decreases exponentially from 0.75 to 0.44, as shown in Figure 10(c). The CaO content in the slag decreases with the increase of Fe_2O_3 addition amount in the slag, leading to the equilibrium mass fraction of C_2S gradually is decreased and its phosphorus enrichment capacity is weakened. The increase of Fe_2O_3 addition amount improves the dephosphorization ability of the multiphase dephosphorization slag from the perspective of increasing the oxygen potential of the slag–hot metal interface.

Figure 10(d) shows that with the initial P content of hot metal increasing from 0.057 to 0.292 pct, R_{CS} increases linearly from 0.42 to 0.57, and R_{C_2S} decreases linearly from 0.56 to 0.41. The phosphorus potential of the slag–hot metal interface increases with the increase of the initial P content of hot metal, which can drive the dephosphorization reaction forward. CaO and FeO in slag are continuously consumed with the increase of initial P content in hot metal by dephosphorization reaction, which is proved by the decrease of slag basicity and FeO content. As a result, the phosphorus enrichment capacity of CS increases, while that of C_2S decreases. The effect of reaction time on the phosphorus enrichment contribution ratio of calcium silicate in multiphase dephosphorization slag is similar to that of temperature. With increasing time, the dephosphorization slag gradually melts from the hard shell shape to the molten state, the SiO_2 content in the slag gradually increases and the slag basicity decreases from 1.62 to 1.32. Multiphase dephosphorization slag tends to form CS with increasing time, which leads to the increase and decrease of the phosphorus enrichment contribution ratio of CS and C_2S, respectively. It can be seen from Figure 10(e) that with the initial P content of hot metal increasing from 0.057 to 0.292 pct, R_{CS} increases exponentially from 0.36 to 0.56, while R_{C_2S} decreases exponentially from 0.62 to 0.43. Table V lists the change trend of phosphorus enrichment contribution ratio of four kinds of calcium silicate in multiphase dephosphorization slag under different process parameters.

The correlation degree between the process parameters and the phosphorus enrichment ability of calcium silicate is further studied. The correlation coefficients δ between the phosphorus enrichment contribution ratio of four kinds of calcium silicate and different process parameters are calculated with Pearson Product–Moment Correlation Coefficient (PPMCC). In the field of natural science, the PPMCC is widely used to measure the correlation between two variables.[65] The closer is the calculated δ value to $\pm$ 1, the higher is the correlation between the phosphorus enrichment contribution ratio of a certain kind of calcium silicate and the process parameter. The equation of sample PPMCC is shown in Eq. [12],[66] where x_i and y_i are sample values of two variable arrays, and n is the number of samples.

$$\delta_{xy} = \frac{n\sum x_i y_i - \sum x_i \sum y_i}{\sqrt{n\sum x_i^2 - (\sum x_i)^2}\sqrt{n\sum y_i^2 - (\sum y_i)^2}}. \quad [12]$$

Figure 11(a) shows the correlation coefficient between the phosphorus enrichment contribution ratio of four kinds of calcium silicate in multiphase dephosphorization slag and the process parameters, and Figure 11(b) shows the rankings of absolute values of correlation coefficients between the phosphorus enrichment contribution ratio of different calcium silicates in multiphase dephosphorization slag and the process parameters. Combined with Figures 11(a) and (b), it can be seen that the slag basicity and R_{CS} and R_{C_2S} have the highest absolute values of correlation coefficient $|\delta|$, which can reach more than 0.99. The $|\delta|$ between the five process parameters and the R_{CS}, R_{C_2S} and R_{C_3S} can reach more than 0.8, which indicates that they have strong correlation, and the change of process parameters can significantly affect the phosphorus enrichment contribution ratio of CS, C_2S and C_3S. The $|\delta|$ between $R_{C_3S_2}$ and process parameters are concentrated at the end of the ranking range. The $|\delta|$ between temperature, Fe_2O_3 addition amount, initial P content of hot metal and time and $R_{C_3S_2}$ are between 0.3 and 0.8, showing weak correlation. The $|\delta|$ between the slag basicity and $R_{C_3S_2}$ is the lowest, only 0.04, which indicates that there is no correlation between them.

D. *Clarify the Phosphorus Enrichment Degree of P_2O_5 Containing Solid Solution in Multiphase Dephosphorization Slag Under Different Process Parameters*

Based on the discussion in Sects. 3.1 and 3.3, it is necessary to clarify the phosphorus enrichment degree of P_2O_5 containing solid solution in multiphase dephosphorization slag for determining the influence of process

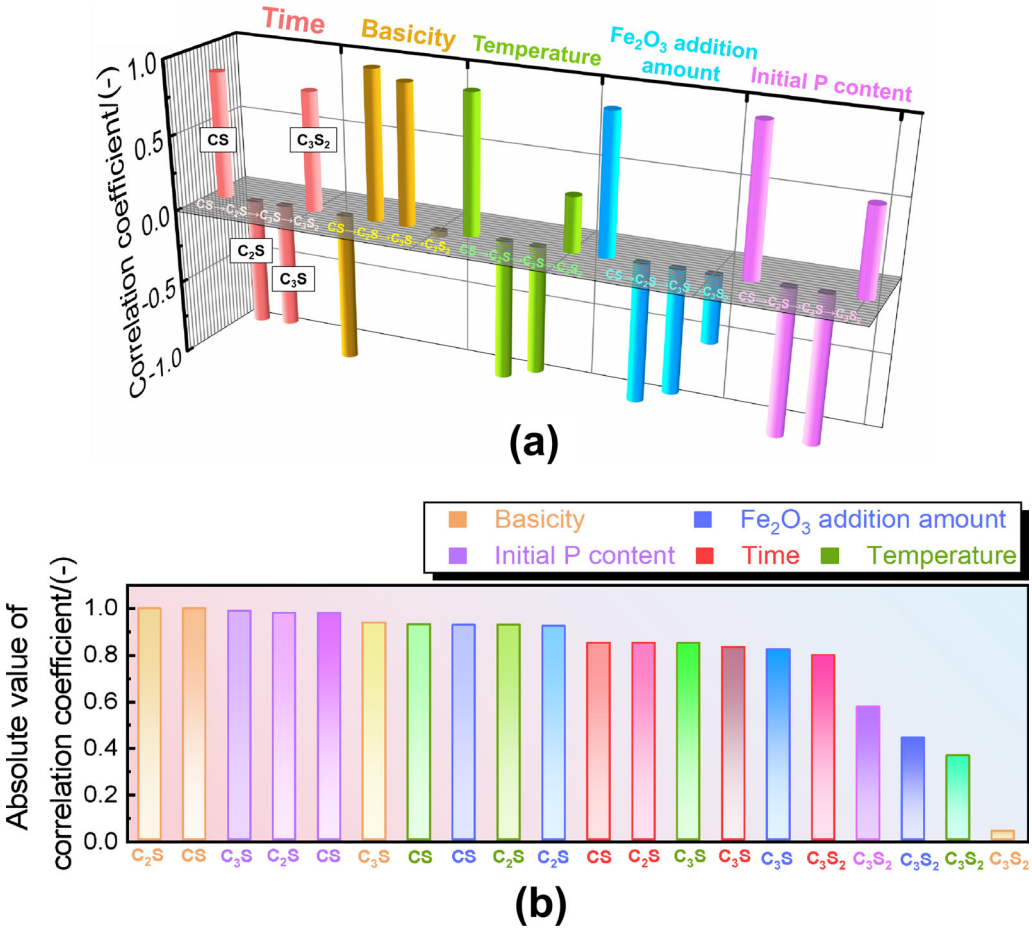

Fig. 11—(*a*) Correlation coefficient between the phosphorus enrichment contribution ratio of four kinds of calcium silicate in multiphase dephosphorization slag and the process parameters, and (*b*) rankings of absolute values of correlation coefficients $|\delta|$ between the phosphorus enrichment contribution ratio of different calcium silicates in multiphase dephosphorization slag and the process parameters.

parameters on the phosphorus enrichment ability of multiphase dephosphorization slag. According to Figures 6 and 10, CS and C_2S are two kinds of calcium silicate with strong reaction ability and high phosphorus enrichment ability in multiphase dephosphorization slag, and the mass action concentration of calcium phosphate (C_iP) in multiphase dephosphorization slag is several orders of magnitude higher than those of other phosphates. Therefore, the present work mainly discusses the phosphorus enrichment degree of P_2O_5 containing solid solution formed by CS, C_2S and calcium phosphate. They can form six P_2O_5 containing solid solutions in the temperature range of 1300 °C to 1450 °C, namely CS–C_2P, CS–C_3P, CS–C_4P, C_2S–C_2P, C_2S–C_3P and C_2S–C_4P.[4,62] The R_{Ci-Pj} defined by IMCT can quantitatively calculate the phosphorus enrichment degree of P_2O_5 containing solid solution in multiphase dephosphorization slag. Taking C_2S–C_3P as an example, $R_{C_2S-C_3P}$ can be calculated by Eq. [13], and the detailed derivation process can be found in our previous paper.[4]

$$R_{C_2S-C_3P} = \frac{\left(N_{C_2S-C_3P}\frac{M_{P_2O_5}}{M_{C_2S-C_3P}}\right)}{\sum\limits_{\substack{i=1-4\\ j=1-7}}\left(N_{Ci-Pj}\frac{M_{P_2O_5}}{M_{Ci-Pj}}\right)}. \quad [13]$$

Table VI enumerates the quantitative calculation results of phosphorus enrichment degree range of P_2O_5 containing solid solution in multiphase dephosphorization slag under different process parameters. Among the six P_2O_5 containing solid solutions studied, the sum of the R_{CS-C_3P} and $R_{C_2S-C_3P}$ is greater than 0.95, which is the two P_2O_5 containing solid solutions with the strongest phosphorus enrichment ability in multiphase dephosphorization slag. The effect of process parameters on the phosphorus enrichment degree of CS–C_3P and C_2S–C_3P in multiphase dephosphorization slag is further studied, and the transformation node of the phosphorus enrichment degree of P_2O_5 containing solid solution in multiphase dephosphorization slag is clarified under different process parameters. Figures 12(a)

Table VI. Quantitative Calculation Results of Phosphorus Enrichment Degree Range of P_2O_5 Containing Solid Solution in Multiphase Dephosphorization Slag Under Different Process Parameters

R_{Ci-Pj}	Slag Basicity (—)	Temperature (°C)	Fe_2O_3 Addition Amount (g)	Initial P Content (Pct)	Time (Min)
CS–C_2P	1.02×10^{-5} to 4.35×10^{-4}	2.40×10^{-6} to 7.25×10^{-5}	1.48×10^{-5} to 1.60×10^{-4}	7.50×10^{-5} to 1.92×10^{-4}	5.23×10^{-5} to 1.77×10^{-4}
CS–C_3P	0.18 to 0.71	0.11 to 0.32	0.21 to 0.54	0.42 to 0.57	0.36 to 0.56
CS–C_4P	2.86×10^{-4} to 8.04×10^{-4}	6.43×10^{-4} to 1.17×10^{-3}	4.52×10^{-4} to 7.69×10^{-4}	4.23×10^{-4} to 5.78×10^{-4}	4.36×10^{-4} to 6.32×10^{-4}
C_2S–C_2P	4.35×10^{-5} to 1.69×10^{-4}	1.85×10^{-5} to 1.45×10^{-4}	5.12×10^{-5} to 1.29×10^{-4}	1.00×10^{-4} to 1.37×10^{-4}	8.72×10^{-5} to 1.33×10^{-4}
C_2S–C_3P	0.28 to 0.78	0.65 to 0.85	0.44 to 0.75	0.41 to 0.56	0.43 to 0.62
C_2S–C_4P	1.15×10^{-4} to 3.52×10^{-3}	2.40×10^{-3} to 5.11×10^{-3}	3.76×10^{-4} to 2.74×10^{-3}	3.10×10^{-4} to 7.94×10^{-3}	3.38×10^{-4} to 1.09×10^{-3}

through (e) shows the change in phosphorus enrichment degree of CS–C_3P and C_2S–C_3P in multiphase dephosphorization slag with basicity, temperature, Fe_2O_3 addition amount, initial P content of hot metal and time, respectively. Figure 12(f) shows the effect of slag basicity of selected all data from multiple process parameters on phosphorus enrichment degree of C_2S–C_3P.

It can be seen from Figure 12(a) that with increasing slag basicity, R_{CS-C_3P} decreases linearly and $R_{C_2S-C_3P}$ increases linearly. When the slag basicity exceeds 1.45, C_2S–C_3P replaces CS–C_3P as the P_2O_5 containing solid solution with the strongest phosphorus enrichment capacity in the multiphase dephosphorization slag. Figure 12(b) shows that the R_{CS-C_3P} increases linearly with increasing temperature, while that of $R_{C_2S-C_3P}$ decreases linearly. In the temperature range of 1300 °C to 1450 °C, the $R_{C_2S-C_3P}$ is always higher than that of R_{CS-C_3P}, which is caused by the higher slag basicity. With increasing Fe_2O_3 addition amount, R_{CS-C_3P} increases exponentially, while $R_{C_2S-C_3P}$ decreases exponentially, as shown in Figure 12(c). When the Fe_2O_3 addition amount reaches 19.55 g, the phosphorus enrichment degree of CS–C_3P increases to the same level as that of C_2S–C_3P. With further increasing Fe_2O_3 addition amount to 30 g, CS–C_3P begins to become the P_2O_5 containing solid solution with the strongest phosphorus enrichment capacity in the multiphase dephosphorization slag.

In Figure 12(d), with increasing initial P content in hot metal, R_{CS-C_3P} increases linearly, while $R_{C_2S-C_3P}$ decreases linearly. When the main P_2O_5 containing solid solution in multiphase dephosphorization slag changes from C_2S–C_3P to CS–C_3P, the initial P content of hot metal is 0.183 pct. Figure 12(e) shows that R_{CS-C_3P} increases exponentially and $R_{C_2S-C_3P}$ decreases exponentially with increasing time. After 8.46 minutes of dephosphorization reaction, the phosphorus enrichment degree of CS–C_3P exceeds that of C_2S–C_3P, and CS–C_3P occupies the dominant position of phosphorus enrichment capacity in multiphase dephosphorization slag. It can be seen from Figure 12(f) that with the slag basicity increasing from 1 to 2.2, the phosphorus enrichment degree of C_2S–C_3P increases linearly. The mathematical relationship between slag basicity and phosphorus enrichment degree of C_2S–C_3P is shown in Eq. [14], and the fitting coefficient is 0.92, which shows that the slag basicity under different process parameters has a significant linear relationship with the phosphorus enrichment degree of C_2S–C_3P, and their relationship is not affected with changing process parameters. The slag basicity can determine the type of calcium silicate formed in the multiphase dephosphorization slag, and further affect the change of phosphorus enrichment degree of P_2O_5 containing solid solution in the multiphase dephosphorized slag.

$$R_{C_2S-C_3P} = 0.500B - 0.228, \quad r^2 = 0.92. \qquad [14]$$

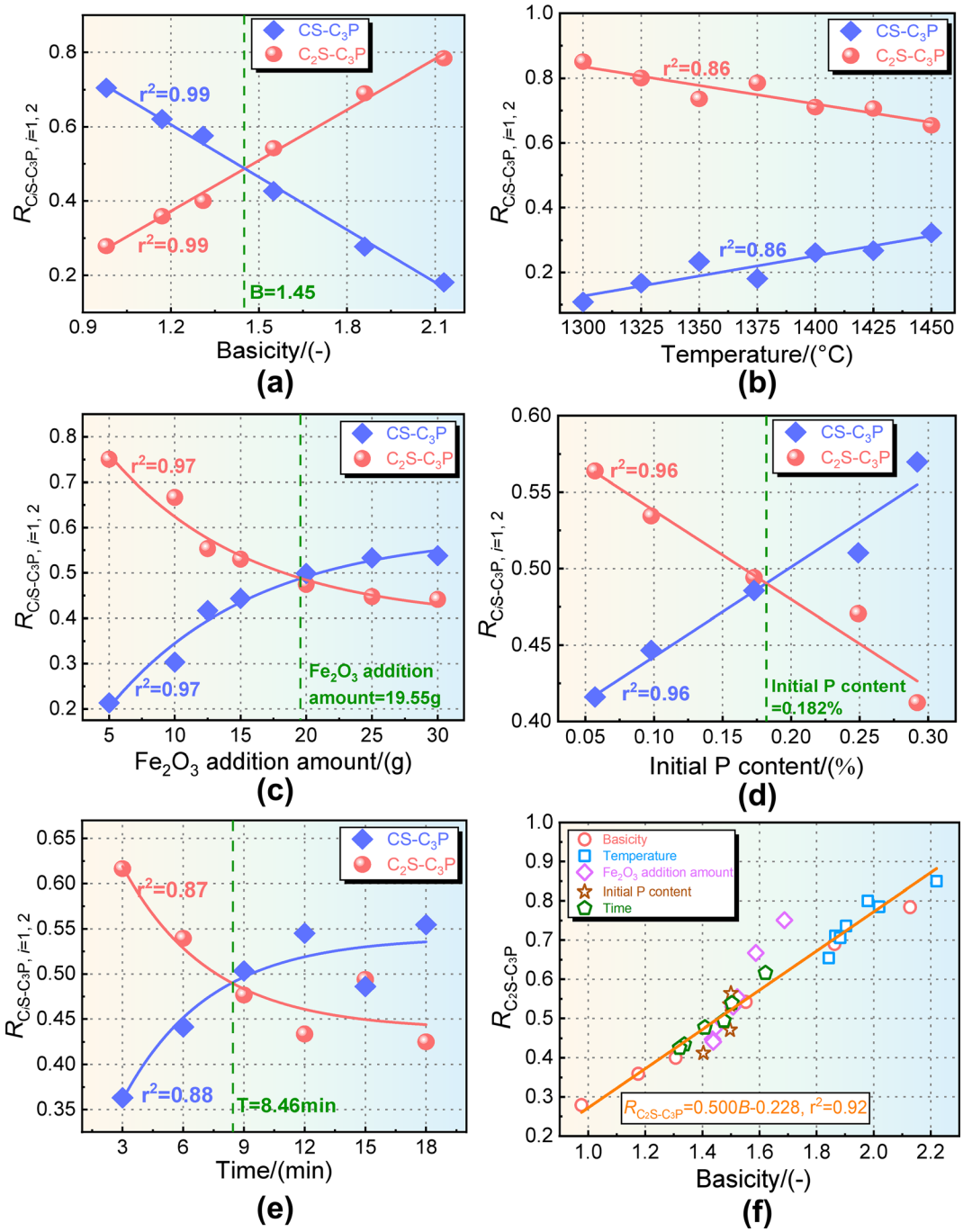

Fig. 12—Changes in phosphorus enrichment degree of CS–C_3P and C_2S–C_3P in multiphase dephosphorization slag with (*a*) basicity, (*b*) temperature, (*c*) Fe_2O_3 addition amount, (*d*) initial P content and (*e*) time, and (*f*) effect of slag basicity of selected all data from multiple process parameters on phosphorus enrichment degree of C_2S–C_3P.

E. *Consistency of the Phosphorus Enrichment Contribution Ratio of Calcium Silicate Calculated Based on IMCT and the Coefficient n of C_nS–C_3P Measured Based on Laboratory Experiments*

According to IMCT calculation results, the phosphorus enrichment degree of CS–C_3P and C_2S–C_3P is several orders of magnitude higher than the P_2O_5 containing solid solution formed by other phosphates and calcium silicate. Therefore, the present work assumes that phosphate in multiphase dephosphorization slag mainly exists in the form of C_3P, and further estimates the coefficient n of C_nS–C_3P in multiphase dephosphorization slag. Based on the above premise, the sum of the mass fractions of CaO, SiO_2 and P_2O_5 in the multiphase dephosphorization slag represents the total mass fraction of C_nS–C_3P formed in the multiphase dephosphorization slag. The mass fraction of CaO required to combine with P_2O_5 to form C_3P is calculated with Eq. [15-1], and the coefficient n of C_nS–C_3P in the multiphase dephosphorization slag is

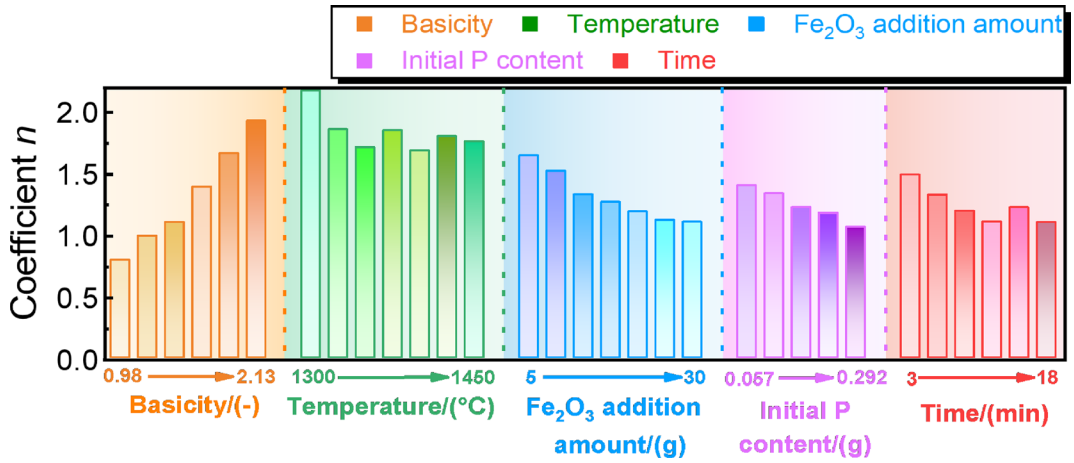

Fig. 13—Estimation results of coefficient n of C_nS–C_3P in multiphase dephosphorization slag under multiple process parameters.

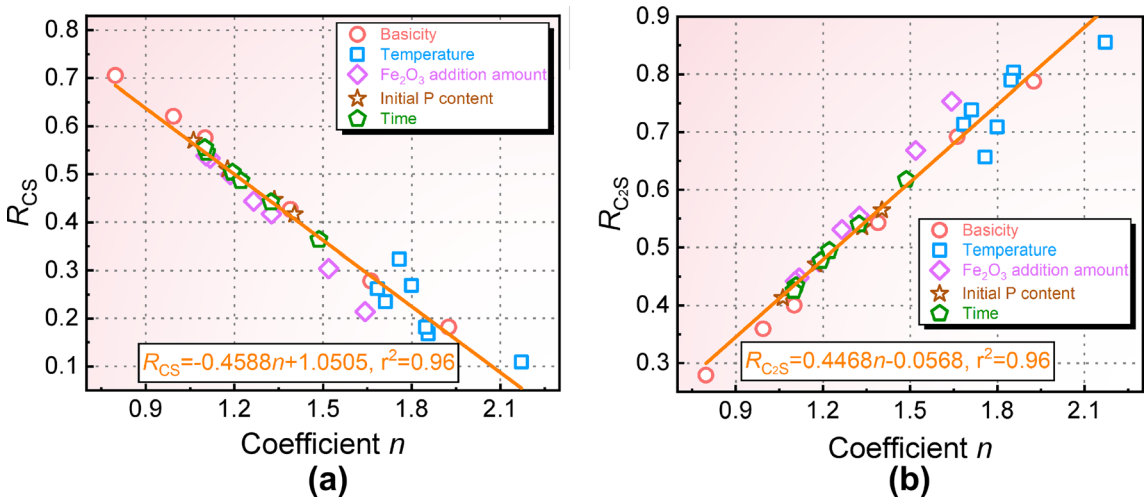

Fig. 14—Relationship between the phosphorus enrichment contribution ratios of (*a*) CS and (*b*) C_2S calculated with IMCT and the coefficient n of C_nS–C_3P in multiphase dephosphorization slag measured with experiment.

roughly calculated with Eq. [15-2]. Figure 13 arranges the estimation results of coefficient n of C_nS–C_3P in multiphase dephosphorization slag under multiple process parameters.

$$m_{CaO}^{C_3P} = 3 \times \frac{m_{P_2O_5}^{Slag}}{M_{P_2O_5}} \times M_{CaO}, \qquad [15-1]$$

$$n = \frac{m_{CaO} - m_{CaO}^{C_3P}}{M_{CaO}} \Big/ \frac{m_{SiO_2}}{M_{SiO_2}}. \qquad [15-2]$$

It can be seen from Figure 13 that with increasing slag basicity, the coefficient n of C_nS–C_3P in multiphase dephosphorization slag increases reasonably. The increases of Fe_2O_3 addition amount, the initial P content of hot metal and time will reduce the coefficient n of C_nS–C_3P in multiphase dephosphorization slag. In the temperature range of 1300 °C to 1450 °C, the coefficient n of C_nS–C_3P in multiphase dephosphorization slag fluctuates between 1.68 and 2.17. The coefficient n of C_nS–C_3P in multiphase dephosphorization slag is concentrated in the range of 0.8 to 2.2 under different process parameters, which indicates that the P_2O_5 containing solid solutions formed in multiphase dephosphorization slag are mainly CS–C_3P and C_2S–C_3P. This result is consistent with the result calculated with IMCT that the main P_2O_5 containing solid solutions in multiphase dephosphorization slag. The slag basicity has the most obvious influence on coefficient n of C_nS–C_3P in multiphase dephosphorization slag, because the change of slag basicity will directly affect CaO/SiO_2 value in slag.

R_{CS} and R_{C_2S} calculated with IMCT under the different parameters are juxtaposition fitted with coefficient n of C_nS–C_3P in multiphase dephosphorization slag measured with experiment under the different parameters, so as to verify the consistency of phosphorus enrichment capacity of calcium silicate in multiphase dephosphorization slag. Figures 14(a) and (b) shows the

relationship between the phosphorus enrichment contribution ratios of CS and C_2S calculated with IMCT and the coefficient n of C_nS–C_3P in multiphase dephosphorization slag measured with experiment. Combined with Figures 14(a) and (b), with the coefficient n increasing from 0.80 to 2.17, the R_{CS} decreases linearly from 0.71 to 0.11, while R_{C_2S} increases linearly from 0.28 to 0.86. Equations [16-1] and [16-2] regress the mathematical relationship between R_{CS}, R_{C_2S} and coefficient n of C_nS–C_3P in multiphase dephosphorization slag, respectively. The fitting coefficients of Eqs. [16-1] and [16-2] are both as high as 0.96, which shows that they have a good linear relationship without being affected by process parameters.

$$R_{CS} = -0.4588n + 1.0505, \quad r^2 = 0.96, \qquad [16-1]$$

$$R_{C_2S} = 0.4468n - 0.0568, \quad r^2 = 0.96. \qquad [16-2]$$

The above results show that when the main P_2O_5 containing solid solution in the multiphase dephosphorization slag gradually changes from CS–C_3P to C_2S–C_3P, the phosphorus enrichment contribution ratio of C_2S calculated based on IMCT increases significantly, and the phosphorus enrichment contribution ratio of CS can be reasonably reduced. The phosphorus enrichment capacity of calcium silicate in multiphase dephosphorization slag calculated by IMCT is consistent with the variation rule of coefficient n of C_nS–C_3P in multiphase dephosphorization slag measured in the experiment, which indicates that IMCT can correctly predict the phosphorus enrichment capacity of calcium silicate in multiphase dephosphorization slag under different process parameters. IMCT provides a reliable and accurate thermodynamic method for studying the phosphorus enrichment capacity of calcium silicate in low temperature and low basicity multiphase dephosphorization slag.

IV. CONCLUSIONS

In the present work, the phosphorus enrichment capacity of four kinds of calcium silicate in multiphase dephosphorization slag under different process parameters is studied by combining laboratory high temperature experiments and IMCT. The phosphorus enrichment contribution ratio of calcium silicate and phosphorus enrichment degree of P_2O_5 containing solid solution in multiphase dephosphorization slag under different slag basicities, temperatures, Fe_2O_3 addition amounts, initial P contents of hot metal and reaction times are clarified. The consistency of the phosphorus enrichment capacity of calcium silicate in multiphase dephosphorization slag based on laboratory measurement and IMCT thermodynamic calculation is verified. The following conclusions are obtained:

(1) Dephosphorization ratio is enhanced by increasing the slag basicity, Fe_2O_3 addition amount and dephosphorization time. With increasing temperature and initial P content of hot metal, dephosphorization ratio increases first and then decreases. Among the five process parameters that affect the dephosphorization of hot metal, the Fe_2O_3 addition amount has the most obvious effect on the dephosphorization ratio of hot metal, while the initial P content of hot metal has the smallest effect on the dephosphorization ratio of hot metal.
(2) The mass action concentration of simple components in multiphase dephosphorization slag, such as CaO and SiO_2, and complex components, such as C_2S and C_3P, can change regularly with the change of process parameters. The mass action concentration of FeO in multiphase dephosphorization slag is exponential positive correlation with its mass fraction, and the relationship between them is not affected by process parameters. Increasing the content of basic oxides can improve the reaction capacity of O^{2-} in multiphase dephosphorization slag under different process parameters.
(3) The phosphorus enrichment contribution ratio of CS and C_2S in multiphase dephosphorization slag exceeds 95 pct. The phosphorus enrichment contribution ratio of C_2S is negatively related to temperature, Fe_2O_3 addition amount, initial P content of hot metal and time in varying degrees, and positively related to the slag basicity. The change rule of phosphorus enrichment contribution ratio of CS is opposite to that of C_2S. The change of process parameters can significantly affect the phosphorus enrichment contribution ratio of CS, C_2S and C_3S by comparing the correlation coefficient δ.
(4) Within the research range of respective process parameters, the transformation nodes of the phosphorus enrichment degree of CS–C_3P and C_2S–C_3P in multiphase dephosphorization slag are as follows: the slag basicity is 1.45, the Fe_2O_3 addition amount is 19.55 g, the initial P content of hot metal is 0.182 pct and the reaction time is 8.46 minutes. In the temperature range of 1300 °C to 1450 °C, the phosphorus enrichment degree of C_2S–C_3P is always higher than that of CS–C_3P, which is caused by the higher slag basicity.
(5) The phosphorus enrichment capacity of calcium silicate in multiphase dephosphorization slag calculated by IMCT is consistent with the variation rule of coefficient n of C_nS–C_3P in multiphase dephosphorization slag measured in the experiment, which indicates that IMCT can correctly predict the phosphorus enrichment capacity of calcium silicate in multiphase dephosphorization slag under different process parameters.

ACKNOWLEDGMENTS

The authors gratefully acknowledge financial support by the National Natural Science Foundation of China (U1960202).

CONFLICT OF INTEREST

On behalf of all authors, the corresponding author states that there is no conflict of interest.

REFERENCES

1. J. Diao, W. Zhou, Z.Q. Ke, Y. Qiao, T. Zhang, X. Liu, and B. Xie: *J. Clean. Prod.*, 2016, vol. 125, pp. 159–67.
2. J.L. Guo, Y.P. Bao, and M. Wang: *Waste Manag.*, 2018, vol. 78, pp. 318–30.
3. H. Sun, J. Yang, X.W. Lu, W.S. Liu, G.F. Ye, R.H. Zhang, and W.K. Yang: *Metals*, 2021, vol. 11, p. 1030.
4. H. Sun, J. Yang, R.H. Zhang, and W.K. Yang: *Metall. Mater. Trans. B*, 2021, vol. 52B, pp. 3403–22.
5. W.H. Lin, S.Q. Jiao, K.X. Zhou, J.K. Sun, X.M. Feng, and Q. Liu: *Front. Mater.*, 2020, vol. 7, p. 602522.
6. Y. Wang, S.F. Yang, J.S. Li, J. Feng, and F. Wang: *High Temp. Mater. Proc.*, 2018, vol. 37, pp. 625–33.
7. S.L. Xie, W.L. Wang, D.Y. Huang, H.C. Li, and Y. Du: *Steel Res. Int.*, 2018, vol. 89, p. 1700317.
8. Y.I. Uchida, N. Sasaki, and Y. Miki: *ISIJ Int.*, 2018, vol. 58, pp. 869–75.
9. S.L. Xie, W.L. Wang, Z.H. Pan, H.C. Li, D.Y. Huang, and Y. Du: *Steel Res. Int.*, 2018, vol. 89, p. 1700516.
10. J.Y. Li, M. Zhang, M. Guo, and X.M. Yang: *High Temp. Mater. Proc.*, 2018, vol. 37, pp. 477–86.
11. B. Li, L. Li, H.J. Guo, J. Guo, S.C. Duan, and W.X. Sun: *Ironmak. Steelmak.*, 2020, vol. 47, pp. 771–80.
12. C. Su, N.N. Lv, J.X. Yang, L.S. Wu, H.C. Wang, and Y.C. Dong: *J. Iron Steel Res. Int.*, 2019, vol. 26, pp. 42–51.
13. M.L. Wang and W.Y. Yang: *Ironmak. Steelmak.*, 2020, vol. 47, pp. 1127–34.
14. L.J. Yao, R. Zhu, K. Dong, G.S. Wei, F. Zhao, and Y.X. Tang: *Ironmak. Steelmak.*, 2021, vol. 48, pp. 180–90.
15. C.V. Silva, F.C. Broseghini, E. Junca, F.F. Grillo, and J.R. de Oliveira: *J. Mater. Res. Technol.*, 2020, vol. 9, pp. 10529–36.
16. L. Lin, Y.Q. Liu, J.G. Zhi, S. He, X. Li, Z.X. Hou, and L.Q. Zhang: *Ironmak. Steelmak.*, 2021, vol. 48, pp. 334–42.
17. G.F. Ye, J. Yang, R.H. Zhang, W.K. Yang, and H. Sun: *Int. J. Miner. Metall. Mater.*, 2021, vol. 28, pp. 66–75.
18. W.K. Yang, J. Yang, Y.Q. Shi, Z.J. Yang, F.B. Gao, R.H. Zhang, and G.F. Ye: *Ironmak. Steelmak.*, 2021, vol. 48, pp. 69–77.
19. Z.W. Yan, Z.Y. Deng, and M.Y. Zhu: *Metall. Mater. Trans. B*, 2021, vol. 52B, pp. 2806–15.
20. R.M. de Souza, V. Andreatta, I.A.S. Santos, E. Junca, F.F. Grillo, and J.R. de Oliveira: *J. Mater. Res. Technol.*, 2021, vol. 15, pp. 5307–15.
21. N. Maruoka and H. Kubo: *ISIJ Int.*, 2021, vol. 61, pp. 2220–26.
22. N. Kikuchi, A. Matsui, and Y. Uchida: *ISIJ Int.*, 2020, vol. 60, pp. 922–29.
23. W.K. Yang, J. Yang, Y.Q. Shi, Z.J. Yang, F.B. Gao, R.H. Zhang, and G.F. Ye: *Steel Res. Int.*, 2021, vol. 92, p. 2000438.
24. W.K. Yang, J. Yang, R.H. Zhang, and H. Sun: *ISIJ Int.*, 2021, vol. 61, pp. 2490–2500.
25. W.K. Yang, J. Yang, Y.Q. Shi, Z.J. Yang, F.B. Gao, R.H. Zhang, and H. Sun: *Metals*, 2021, vol. 11, p. 417.
26. R.H. Zhang, J. Yang, W.K. Yang, and H. Sun: *Ironmak. Steelmak.*, 2021, vol. 48, pp. 1277–90.
27. R.H. Zhang, J. Yang, H. Sun, and W.K. Yang: *Steel Res. Int.*, 2021, vol. 92, p. 2100256.
28. W.K. Yang, J. Yang, R.H. Zhang, and H. Sun: *Steel Res. Int.*, 2021, vol. 92, p. 2100066.
29. W.K. Yang, J. Yang, R.H. Zhang, H. Sun, and Y.L. Qiu: *Metals*, 2021, vol. 11, p. 1480.
30. W.K. Yang, R.H. Zhang, H. Sun, and J. Yang: *Steel Res. Int.*, 2022, vol. 93, p. 2100378.
31. H.M. Xue, J. Li, X.J. Xia, Y. Wan, L.J. Chen, and C.J. Lv: *Trans Indian Inst. Met.*, 2021, vol. 74, pp. 1655–61.
32. Z.L. Wang, Y.P. Bao, and D.Z. Wang: *C. G and M. Wang: Crystals*, 2022, vol. 12, pp. 1030–40.
33. G.B. Sun and X.D. Xiang: *Metals*, 2022, vol. 12, p. 751.
34. R.H. Zhang, J. Yang, W.K. Yang, and H. Sun: *Metall. Mater. Trans. B*, 2022, vol. 53B, pp. 3013–24.
35. J.L. Sun, C.J. Liu, and M.F. Jiang: *ISIJ Int.*, 2022, vol. 62, pp. 515–23.
36. H. Sun, J. Yang, R.H. Zhang, and W.K. Yang: *ISIJ Int.*, 2022, vol. 62, pp. 1078–90.
37. X.H. Huang: *Principles of Iron and Steel Metallurgy*, Metallurgical Industry Press, Beijing, 2002.
38. T. Hamano, S. Fukagai, and F. Tsukihashi: *ISIJ Int.*, 2006, vol. 46, pp. 490–95.
39. D. Cédric, B. Christine, V. Emmanuel, A. Mathieu, F. Franck, F. Bodénan, and P. Jacques: *Cem. Concr. Res.*, 2015, vol. 73, pp. 207–14.
40. M. Zhong, H. Matsuura, and F. Tsukihashi: *ISIJ Int.*, 2015, vol. 55, pp. 2283–88.
41. M. Zhong, H. Matsuura, and F. Tsukihashi: *Mater. Trans.*, 2015, vol. 56(8), pp. 1192–98.
42. M. Zhong, H. Matsuura, and F. Tsukihashi: *Metall. Mater. Trans. B*, 2016, vol. 47B, pp. 1745–52.
43. C. Borgianni and P. Granati: *Metall. Trans. B*, 1977, vol. 8B, pp. 147–51.
44. M. Hillert, B. Jansson, B. Sundman, and J. Ågren: *Metall. Trans. A*, 1985, vol. 16A, pp. 261–66.
45. R. Schmid and Y.A. Chang: *Calphad*, 1985, vol. 9, pp. 363–82.
46. G.G. Cheng, J. Zhang, and P. Zhao: *Acta Metall. Sin. Engl. Lett.*, 1997, vol. 10, pp. 17–21.
47. J. Zhang: *Acta Metall. Sin. Engl. Lett.*, 2001, vol. 14, pp. 177–90.
48. J. Zhang: *Computational Thermodynamics of Metallurgical Melt and Solutions*, Metallurgical Industry Press, Beijing, 2007.
49. A.D. Pelton, S.A. Degterov, G. Eriksson, C. Robelin, and Y. Dessureault: *Metall. Mater. Trans. B*, 2000, vol. 31B, pp. 651–59.
50. A.D. Pelton and P. Chartrand: *Metall. Mater. Trans. B*, 2001, vol. 32B, pp. 1355–60.
51. P. Chartrand and A.D. Pelton: *Metall. Mater. Trans. B*, 2001, vol. 32B, pp. 1397–1407.
52. A.D. Pelton, P. Chartrand, and G. Eriksson: *Metall. Mater. Trans. B*, 2001, vol. 32B, pp. 1409–16.
53. S. Ban-ya: *ISIJ Int.*, 1993, vol. 33, pp. 2–11.
54. J. Bygden, D. Sichen, and S. Seetharaman: *Steel Res.*, 1994, vol. 65, pp. 421–28.
55. S. Basu, A.K. Lahiri, and S. Seetharaman: *Metall. Mater. Trans. B*, 2008, vol. 39B, pp. 447–56.
56. P. Fredriksson and S. Seetharaman: *Steel Res. Int.*, 2004, vol. 75, pp. 357–65.
57. D.P. Tao: *Metall. Mater. Trans. B*, 2006, vol. 37B, pp. 1091–97.
58. D.P. Tao: *J. Mater. Sci. Technol.*, 2008, vol. 24, pp. 797–802.
59. L. Zhang, S. Sun, and S. Jahanshahi: *J. Phase Equilib. Diffus.*, 2007, vol. 28, pp. 121–29.
60. X.M. Yang, J.S. Jiao, R.C. Ding, C.B. Shi, and H.J. Guo: *ISIJ Int.*, 2009, vol. 49, pp. 1828–37.
61. X.M. Yang, J.P. Duan, C.B. Shi, M. Zhang, Y.L. Zhang, and J.C. Wang: *Metall. Mater. Trans. B*, 2011, vol. 42B, pp. 738–70.
62. J.Y. Li, M. Zhang, M. Guo, and X.M. Yang: *Metall. Mater. Trans. B*, 2014, vol. 45B, pp. 1666–82.
63. H. Sun, J. Yang, W.K. Yang, and R.H. Zhang: *Metall. Mater. Trans. B*, 2023, vol. 54B, pp. 115–45.
64. H. Sun, J. Yang, W.K. Yang, and R.H. Zhang: *Steel Res. Int.*, 2022. https://doi.org/10.1002/srin.202200662.
65. A.J. Bishara and J.B. Hittner: *Psychol. Methods*, 2012, vol. 17, pp. 399–417.
66. D. Wang: *Probability Theory and Mathematical Statistics*, Beijing Institute of Technology Press, Beijing, 2020.